Eindhoven University of Technology

MASTER

Organic electronic ratchet devices : exploring the electronic ratchet and investigating a solar ratchet

Janssen, N.M.A.

Award date:
2013

Link to publication

Master thesis
Research group Molecular Materials and Nanosystems
Department of Applied Physics
Eindhoven University of Technology

Organic Electronic Ratchet Devices

Exploring the electronic ratchet and investigating a solar ratchet

N.M.A. Janssen

August 2013

Supervisor:
dr. ir. M. Kemerink

 Graduation commission:
dr. ir. M. Kemerink
prof. dr. ir. R.A.J. Janssen
prof. dr. ir. O.J. Luiten
prof. dr. ir. H.J.M. Swagten

1 Abstract

This thesis reports on the investigation of two related topics, the (in)-organic electronic ratchet and the organic solar ratchet. These are two implementations of the electronic ratchet device that will first be introduced.

The electronic ratchet generates electrical current and voltage by rectifying an external perturbation, in the present case an oscillating voltage. The oscillation is rectified by a periodic, asymmetric potential in which electronic charges are placed. The external perturbation drives the system away from equilibrium, causing detailed balance to be broken; consequently the periodic asymmetry of the potential leads to a net motion of the charges, comparable to the net motion of marbles on a shaking washboard. Note that under equilibrium conditions no (spontaneous) current will flow in any potential.

In this work we show that the generated current as a function of the frequency of the driving signal can be scaled onto a universal profile, covering many orders of magnitude in frequency. Simulations show that this profile is predominantly dependent on drift (as opposed to diffusion) currents in the ratchet.

Experimentally this is verified by combining measurements on three different disordered semiconducting materials. IGZO (Indium Gallium Zinc Oxide) as an inorganic amorphous electron semiconductor and Pentacene and P3HT/PCBM as organic hole semiconductors. The combined scaled current profile shows a consistent behavior for the three materials over at least seven orders of magnitude of (scaled) frequency.

The solar ratchet is a lateral solar cell which can in lowest order be seen as multiple solar cells in series, which is comparable to a multi-junction tandem solar cell. The goal is to create a large open circuit voltage with the intention to create a more efficient solar cell. Simulation of this device turned out to be troublesome due to numerical problems related to the calculation of diffusion currents and of bimolecular recombination. However the first version of the simulation tool, in which drift and diffusion currents are calculated sequentially, shows the possible behavior of the solar ratchet.

The second version, in which the drift and diffusion currents are simultaneously calculated using the Boltzmann transport equation, predicts the solar ratchet to be non-functional due to zero recombination. However, the depletion length of the recombination zones can be calculated. On basis of this an analogy can be made with the recombination zone in the pn-junction in a conventional tandem solar cell. As the tandem solar cell is known to work the solar ratchet is predicted to work as well.

Experimental proofs of principle of the ratchet solar cell were tried to be made but unfortunately no suitable solar ratchet was produced due to various problems that will be discussed.

2 Table of Contents

3 Organic Electronic Ratchets

3.1 Ratchets

The principle for organic electronic ratchets comes from the idea of harvesting energy from Brownian motion. In 1912 the idea was first proposed by Marian Smoluchowski[1] for a machine to extract energy from a system in thermal equilibrium. The ratchet is shown in Figure 1 in which there are two containers. In one there are paddles and in the other there is a ratchet and a pawl plus spring. The two are connected by a thin axis to which a wire connected to a small mass is attached. The Brownian motion moves the paddles, and through the axis the ratchet also moves. This random motion is rectified by the ratchet because it can only move in one direction. The idea was revolutionary because it would defy the second law of thermodynamics when both compartments are in thermal equilibrium i.e. at equal T. So, where does this go wrong? The Brownian random motion would also lift the pawl and spring, making the device move in both ways. Therefore this device can only do work, i.e. lift the mass, if the two compartments are at different temperatures, $T_1<T_2$. This addition was made and shown to deliver work by Richard Feynman[2].
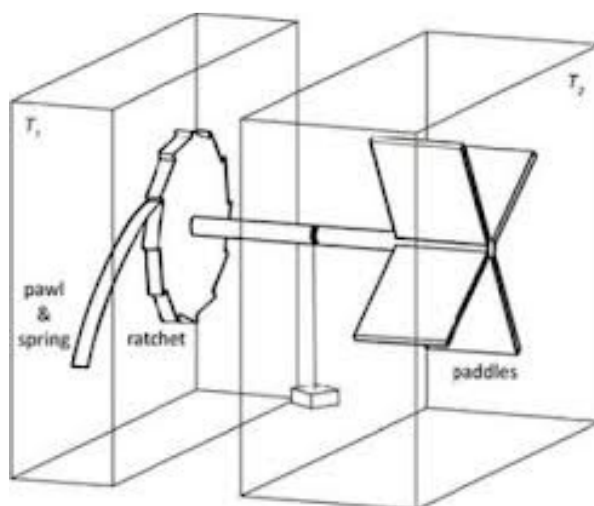
Figure 1 The Feynman-Smoluchowski ratchet. The Brownian motion of the air molecules in the container at T_2 containing the paddles cause the thin axis to turn. In the container at T_1 the motion is limited to a single direction by the ratchet wheel. Hereby upward movement of the small weight on the thin axis is created. This will only work for $T_1<T_2$ because this device needs to obey the first and second law of thermodynamics.[3]

The Feynman-Smoluchowski ratchet harvests energy from random Brownian motion. The next step to the organic electronic ratchets used in this thesis is the on/off ratchet[4]. The working of an on/off ratchet can be seen in Figure 2. It is based on an alternating on and off state. In the on state particles are collected in the minima of an asymmetric potential. When the potential is turned off the particles can diffuse due to the concentration differences centered around the former potential minima. Upon reapplying the potential the particles get trapped again. Due to the asymmetric potential not the same number of particles will travel to either side of the initial minimum.

The description shown here makes no assumptions regarding the nature of the particles, in fact it can be all kinds of particles that diffuse. Displacement of charges, droplets, nano particles, cells, DNA and even marbles is possible. To give an example of an actual working ratchet device we look at the separation of DNA molecules[6].

Figure 3 panel (A) shows the ratchet device with which DNA molecules can be separated with respect to their size. DNA molecules are charged particles with a drift velocity equal for all particles. With the use of an electric field the molecules can be forced through a filter. This filter consists of asymmetric slits as can be seen in panel (B) of Figure 3.

The diffusion coefficient of DNA molecules is dependent on the number of base pairs in the molecule, i.e. its size. Therefore small molecules will have a higher diffusion coefficient which causes a higher percentage of these small molecules to move sideways (upwards in the figure) as can be seen in panel (B) of Figure 3. Combining the asymmetric filter and the molecule size dependent diffusion DNA molecules will be separated with respect to the number of base pairs.
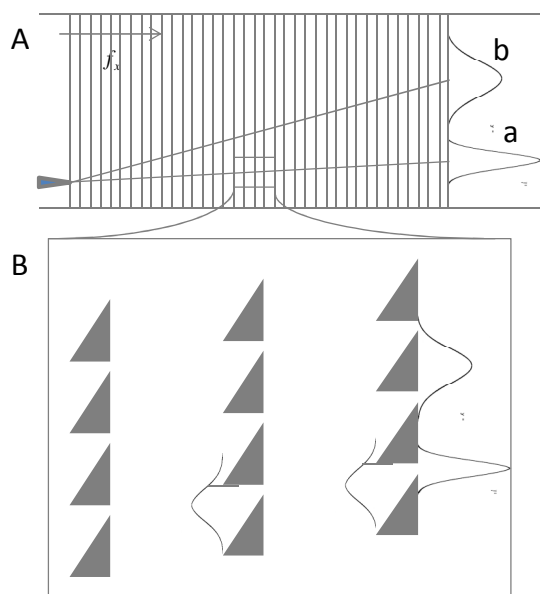
Figure 3 Separation of DNA fragments with respect to the number of base pairs, i.e. size, is done with the device shown in panel (A). An electric field f_x forces the fragments through the device. Separation happens with respect to the diffusion which is different for fragments of size (a) and size (b) in the vertical direction as can be seen in panel (B).

Two implementations of the ratchet concept have been briefly discussed in this introduction. The general principle of the on/off ratchet, and the separation of DNA molecules with different sizes. These implementations are not the only applications[78910] but they give an idea of the vast options the principle of the ratchet as a means to steer the motion of particle gives[11].

Asymmetry is the characteristic that drives the net motion of particles, of any nature, in ratchets. The topic of symmetry will be discussed extensively. In this thesis the topic will be (in)-organic electronic ratchets. This resembles the on/off ratchet in which the ratchet characteristic is formed by the manipulation of the potential landscape in which the charge carriers are transported.

To let the asymmetry of the ratchet work on the particles the system has to be brought out of equilibrium. In the on/off ratchet this is achieved by the potential profile which forces particles to sit at their energy minima. In the DNA separation this is done by the triangular struts which forces particles in a certain position.

3.2 This thesis

Two topics will be discussed in the thesis. First we will look closely at organic electronic flashing ratchets developed by Erik Roeling during his promotion[3]. The main interest will go towards identifying precisely how the current is being transported through the device and how the current reversals that are observed to occur as a function of driving frequency behave. Also the scaling properties of these ratchets will be investigated. The main question for this first part is if these current reversals and the overall behavior are universal for different materials and, if so, how such a scaled picture of a ratchet based on different semiconducting materials look like.

The second topic will be about ratchet solar cells. This novel application uses the characteristics of the ratchet potential to alter the way a tandem solar cell works. It is never used before and therefore highly explorative. The goal for this topic is to check if, and if so how well such a ratchet solar cell could work by using simulations and also by trying to make a working proof of principle.

3.3   Field effect transistor

In the introduction the on/off ratchet has been briefly introduced. However, information is missing to fully understand the concept of the organic electronic ratchet. To start at the basis we have to look at how an organic field effect transistor works and from that point on modify it to turn it into a flashing ratchet. The flashing (in)organic electronic ratchet is the device investigated in the first part of this thesis.

Figure 4 shows the geometry of an organic field effect transistor (OFET), consisting of a source and a drain contact with in between a semiconducting channel on top of a gate dielectric and gate contact stack. The stack formed by the gate electrode, the dielectric and the semiconductor resembles a capacitor, with one of the capacitor plates being the gate and the other the semiconducting channel. For a capacitor the number of charges is equal to $C = {Q}/{V}$ [12].

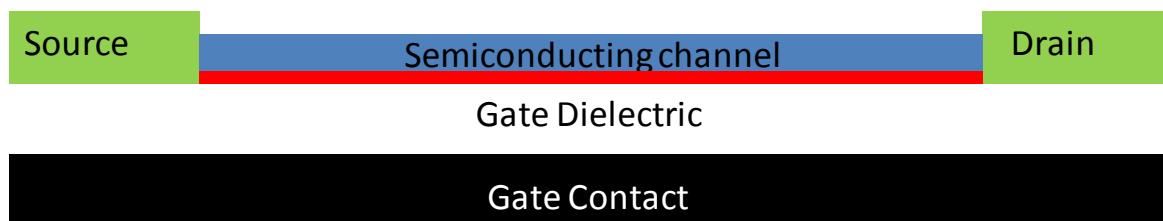| Source	Semiconducting channel	Drain

Gate Dielectric

Gate Contact

Figure 4 Field Effect Transistor. The gate contact is separated from the semiconducting channel by a gate dielectric. By applying a potential to the gate contact charge carriers are introduced in the semiconducting channel depicted in red, forming the accumulation layer. The source and drain contacts are there for making the electronic circuit complete. The charge carriers introduced in the semiconducting channel come from these contacts. The defining characteristic of the transistor is that the source-drain conductivity can be controlled with the gate contact.

Charges are introduced in the semiconducting channel by applying a potential on the gate contact. Figure 5 gives a step by step representation of the band diagram of an OFET at the semiconductor, dielectric and gate interface. For both n- and p-type semiconductors, n for electrons and p for holes, it is shown how the potential of the gate contact results in an accumulation layer being formed in the semiconducting channel. The accumulation layer is represented as the red line in Figure 4.

For n-type semiconductors we can follow the process by investigating the three top panels of Figure 5. The first panel shows the separate energy levels of the semiconductor with a specific Fermi energy, ε_f and the energy level of the gate contact such that flat bands result.

The second panel shows these energy levels when the system is at equilibrium, ε_f is constant throughout the device. Due to the alignment of the Fermi levels band bending occurs at the interface between the semiconductor and the dielectric.

The last panel shows what happens when a potential is applied to the gate contact. The band bending at the interface changes. The Fermi level of the electrons is higher in energy than the electron conducting energy level which results in occupied states in the electron band in which electrons can be transported. These states form the accumulation layer of the OFET.

For a p-type semiconductor the same occurs as can be seen in the bottom row panels.
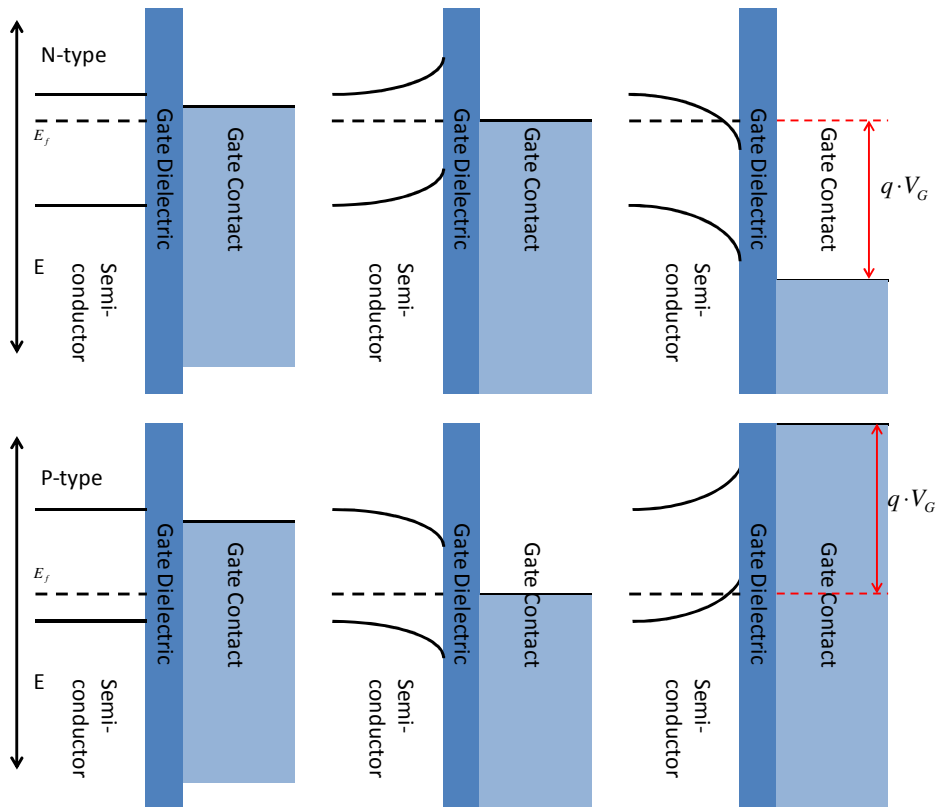
Figure 5 N and P-type band bending in a field effect transistor. The first two panels on the left show the separate energy levels of the field effect transistor. Middle panels show the band bending due to the alignment of the Fermi level ε_f. Right panels show the forming of an accumulation layer due to an applied gate potential.

The transfer curves for these n- and p-type devices are shown in Figure 6. The current as a function of the gate potential is schematically represented. The gate voltage at which the FET is turned on is called the threshold voltage (V_{th})[13]. So far we assumed the threshold voltage is at V_g=0 but this does not need to be. V_{th} is dependent on the Fermi level of the semiconductor and on already existent charge carriers in the channel.

Under prolonged gate bias this threshold voltage can shift which is called the bias stress effect[14]. Trapped charge carriers along with charge carriers moving in the dielectric will (partially) screen the potential of the gate electrode. Hence, it will require higher gate voltages to turn on the OFET.
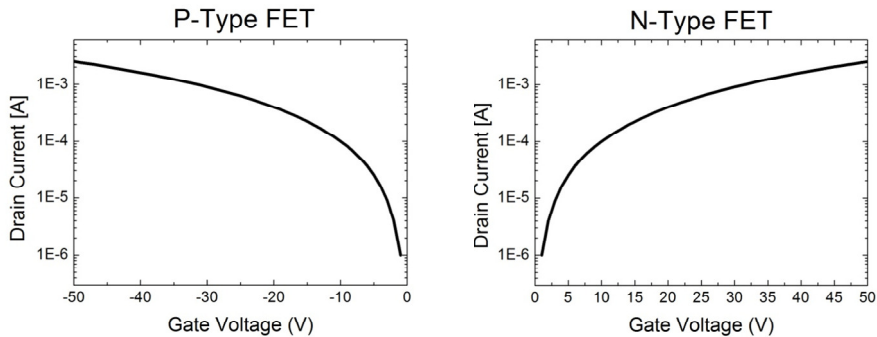
Figure 6 Schematic transfer curves of field effect transistors. The P and N-type OFETs show a current beyond a certain gate voltage chosen to be zero here. The current only flows when the gate voltage creates an accumulation layer in the semiconducting material. The gate voltage at which this occurs is the threshold voltage V_{th}.

3.4 The working of flashing organic electronic ratchets

The field effect transistor geometry is combined with the on/off electronic ratchet. This ratchet has been discussed in the introduction of this thesis. There it was shown that an asymmetric potential is needed along with turning this potential on and off to transport particles over a distance. For this thesis the flashing (organic) electronic ratchet is investigated. We go into the specifics of this ratchet from now on.

In this chapter the flashing organic electronic ratchet is discussed, first the geometric design is shown and evaluated, next the driving signal of the potential applied to the finger electrodes is extensively investigated. Predictions are made regarding the current profiles emerging from the combined geometry and driving signal of the flashing organic electronic ratchet.

3.4.1 Design of flashing ratchet

To thoroughly discuss the topic first the layout of the flashing (organic) electronic ratchet is shown in Figure 7. The top and side views are shown. Starting with the side view, the flashing ratchet is built up on top of a gate electrode (G). In succession several layers are placed on top of each other. First there is a layer of SiO_2 containing finger electrodes (AF1,2). The source (S) and drain (D) contacts are next in line. The (in)-organic semiconductor is deposited on this layer, in this case Pentacene (PEN).

The finger electrodes are interdigitated in an asymmetric manner and, when properly biased, create a potential that is similar to the one shown in the on/off ratchet in Figure 2.

The distance between the source/drain contacts and the first finger pair is b, x, and y are, respectively, the short and long distance between two fingers, L is the repeat length and cl the channel length. All of these lengths are of the scale of micrometers. These parameters are used as the nomenclature for these ratchets, Lx-yPz in which z is the number of finger pairs. For example an L1-8P8 device is a device with short length 1 micron, long length 8 microns and 8 repetitions of the finger electrode pair. The upper panel shows a top view of the device. Notice the large width to length ratio here.
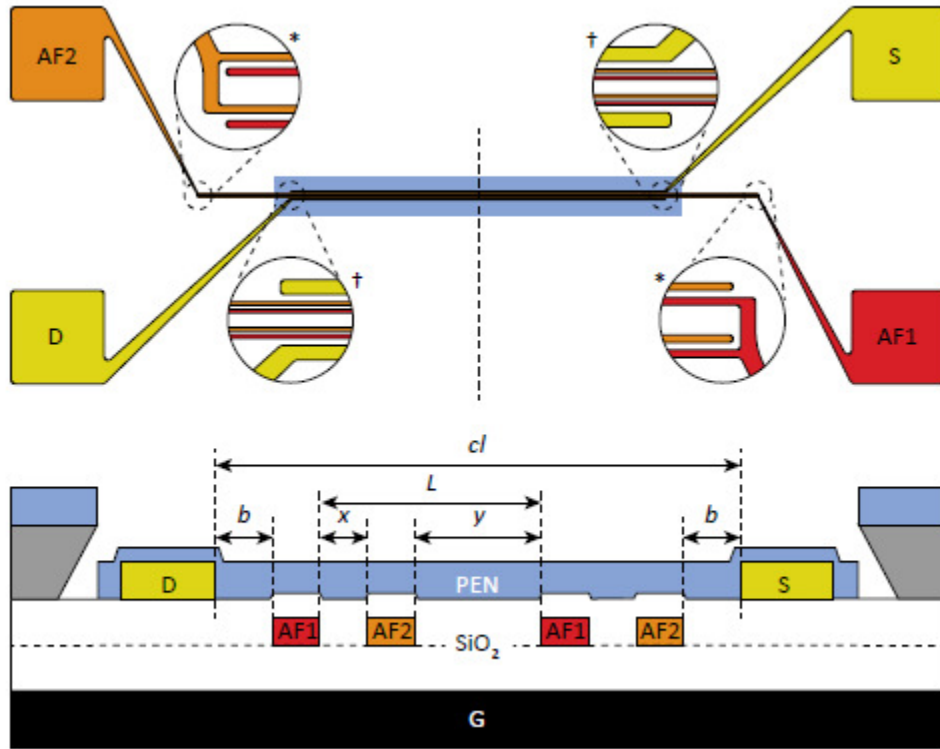
Figure 7 Schematic drawing of the flashing ratchet used in this thesis. The distance between the source/drain contacts and the first finger pairs is *b*, *x* is the short distance between two fingers, *y* the long spacing between finger pairs, L the repeat length and *cl* the channel length. The name for these ratchets comes from this nomenclature, Lx-yPz in which z is the number of finger pairs. *no Pentacene †Pentacene on top of structure.[3]

The design introduced here can be used to create an on/off ratchet. We however stated that a flashing (organic) ratchet is being investigated. The difference comes into play with the way the asymmetric potential is introduced.

Creating an on/off ratchet would require the application of a square wave, Figure 2, to the asymmetric finger electrodes. In frequency space, a square wave is a signal that consists of many sinusoidal components, including many high frequency components. These high frequency components tend to get distorted or lost in the cabling to the ratchet devices and therefore an ill defined input signal will reach the interdigitated finger electrodes.

To circumvent this problem the driving signal will be a simple single sinusoidal wave with a well defined frequency and amplitude.

The analogy between capacitors and OFETs and therefore electronic ratchets also introduces an RC-time which is a typical response time we can now link to this device. Originally this RC-time is the time that it takes for a capacitor *C* to be charged or discharged through a resistor *R*. The RC-times is found to be $L^2/V_g\mu$ [15].

3.4.2 Driving signal

Symmetry breaking and creating an out of equilibrium state are essential to drive current, move a particle or droplet through a ratchet device[16]. A design of such a device has been presented above and also the use of a sinusoidal signal to induce a time dependent potential on the finger electrodes in this design. As a next step we will look thoroughly to the implications of the driving signal.

The on/off ratchet will be used as a start to investigate these implications. The (a)symmetry of an on/off ratchet is related to the spacing of the interdigitated finger electrodes and the potential (differences) applied to the two finger electrodes within one pair which are turned on and off with a certain frequency.

We can make qualitative predictions regarding the dependence of the ratchet current as a function of the driving frequency. If we look at the influence of this frequency we start at extremely low switching frequencies. For these frequencies a small current passes through the device. The drift and diffusion cause the electrons to fully spread over the device. The net current displacement is limited to the displacement upon retrapping the charge carriers while turning on the potential[3].

For medium frequencies a current passes in the exact manner described in Figure 2. Charged carriers pass in the direction determined by the asymmetry and the applied potential. In this case it means that the electrons move to the right, which means overcoming the short distance *x* between the finger electrodes.

For very high frequencies no current passes. This is due to the fact that the electrons cannot move fast enough anymore to reach the next potential maximum before the potential is turned on again. Hence, they are retrapped in the original potential minimum.

This rather long description of a very easy principle seems redundant, but it gives a nice handhold when going to more complex behaviors. In the next few subparagraphs the driving signals are introduced that are used in this thesis. Multiple symmetries will be involved in these signals creating complex behavior.

3.4.2.1   *Transistor drive*
Figure 8 shows the driving signals used in the ratchet system introduced in Figure 7. It shows four different driving signals used to investigate the electronic behavior of organic electronic ratchets. First we look at the Transistor drive. The finger electrodes sit at half the distance from the channel as the gate. Therefore half the gate voltage V_g is applied to these electrodes to create an accumulation layer with a constant density so that properties such as mobility of charge carriers and the threshold voltage can be determined.
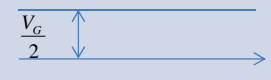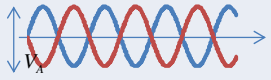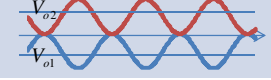
Drive	$V_{AF1}(t)$	$V_{AF2}(t)$	
Transistor (DC)	$\dfrac{V_G}{2}$	$\dfrac{V_G}{2}$	
Symmetric (AC)	$V_{o1}+V_A\cdot\sin(2\cdot\pi\cdot\omega)$	$V_{o2}+V_A\cdot\sin(2\cdot\pi\cdot\omega-\varphi)$	$V_{o1}=V_{o2}$
Reversed (AC)	$V_{o1}+V_A\cdot\sin(2\cdot\pi\cdot\omega)$	$V_{o2}+V_A\cdot\sin(2\cdot\pi\cdot\omega+\varphi)$	$V_{o1}<V_{o2}$
Forward (AC)	$V_{o1}+V_A\cdot\sin(2\cdot\pi\cdot\omega)$	$V_{o2}+V_A\cdot\sin(2\cdot\pi\cdot\omega+\varphi)$	$V_{o1}>V_{o2}$

Figure 8 Driving signals used for the finger electrodes AF1 and AF2 in the SiO$_2$. Transistor drive to run the ratchet as an ordinary field effect transistor. The symmetric signal is used to investigate the behavior of phase and inter-finger distance. Forward and reversed are two driving signals which mostly resemble the on/off ratchet when the phase difference is chosen to be π.

3.4.2.2 Symmetric driving signal

The three other driving signals are used to characterize the (in)-organic electronic ratchet. First the devices are subjected to a so-called symmetric driving signal. From Figure 8 we can deduce 4 different parameters for the two sinusoidal waves.

The first parameter is the frequency ω. The signal amplitude V_A is not varied in any of the simulations or experiments. Furthermore the offset values V_{o1} and V_{o2} are the mean potentials of the two sets of finger electrodes. For the symmetric signal these values are equal. Finally the phase difference φ between the signals of finger electrodes AF1 and AF2 can be set arbitrarily. In the 'symmetric drive' asymmetry can be induced by the phase difference and the geometry of the device.

To predict the currents generated by this device we start with the case that the phase φ between the finger electrodes is zero or 180 degrees. In these cases the expected current is zero. For zero degrees the asymmetry of the geometry is lost and no net current is transported through the device. At 180 degrees the changing potential transports charge to one direction for half of the period of the signal. In the other half of the period the current is transported in exactly the opposite direction.

For arbitrary phases between the two signals a net current is expected. There is asymmetry in the system that is not cancelled out over one whole oscillation period. While conceptually easy, asymmetry implies a current through the device, it is still difficult to grasp when a system is symmetric or not.

With a phase difference between zero and 180 degrees the direction of the net current is in the opposite direction compared to the direction of the current when the phase difference is between 180 degrees and 360 degrees. In the first case AF2 lags behind AF1 while in the second case the opposite occurs. This is known as a current reversal, in this case as a function of phase.

When the frequency is increased in the on/off ratchet typically a decline in current was predicted in 3.4.2. This decline was caused by the fact that less charge carriers can reach the next potential maximum to overcome. The charge carriers needed too much time to accomplish this. We now include this effect to a symmetric driving signal.

In this case the system consists of multiple (two for each finger pair) sinusoidal waves with the same frequency. They form an interference pattern over the semiconducting channel. The exact implications of this interference pattern are difficult to predict. However, it is not unlikely that the preferential direction of the resulting current changes as a function of frequency due to the changing interference pattern[17][18][19][20]. A current reversal as a function of frequency.

3.4.2.3 *Reverse and forward driving signals*
The reverse and forward signal only differ from each other in the offset values of the finger electrodes. For one signal AF1>AF2 because *Vo1>Vo2* and vice versa. Therefore only the forward signal is discussed.

For a forward signal the offset between the two finger electrodes is such that the potential of AF1 is always larger than or equal to AF2. We try to identify the currents generated by the device by looking at special cases.

We start at the point where the phase difference is exactly 180 degrees. The time dependent potential created by the forward driving signal resembles the on/off ratchet the most. Figure 2 is now approximated by a signal that is 'on' when the sinus is at its maximum and 'off' when the sinus is at its minimum. The current is now expected to behave as the current in an on/off ratchet.

At other phases between the driving signals the current becomes much harder to predict. Asymmetry is generated in several manners, geometrically and electrically, each of which has its own preferential direction. The (nonlinear) superposition of these contributions to the current determines the current direction. Current reversals occur when the superposition of all the contributions to the current end up with no net current displacement.

The influence of frequency in this case is evaluated in the discussion of experiments.

3.4.3 To conclude
The asymmetrically placed finger electrodes create possibilities to induce asymmetry in a flashing organic electronic ratchet. Applying driving signals on these finger electrodes leads to multiple possibilities to generate currents through the device. These currents are evaluated as a function of the phase and frequency of these driving signals.

3.5 Simulations

Simulations are performed to investigate the driving mechanism behind the current profiles in the phase-frequency measurements which we will see in Figure 12 and onwards. The drift-diffusion equation is the logical start for simulations on this type of ratchet system[3],[16]:

$$\vec{J_p} = q\mu_p p\vec{E} - qD_p\vec{\nabla}p. \tag{1}$$

The current is determined by the sum of drift and diffusion contributions respectively. p is the free hole concentration, J_p the hole current density, D_p the hole diffusion coefficient, $\vec{E}$ the electric field, q the elementary charge and μ_p the hole mobility. When p is substituted by n and the minus sign is changed in a plus sign the drift-diffusion equation for electrons is obtained. The continuity equation is used for charge conservation and is given by:

$$\vec{\nabla} \cdot \vec{J_p} = -q\partial_t p. \tag{2}$$

Coulomb interaction is taken into account by Poisson's equation derived from the Maxwell equations:

$$\vec{\nabla} \cdot \left(\varepsilon_0 \varepsilon_r \vec{\nabla}\phi\right) = -qp \tag{3}$$

in which ε_0 and ε_r stand respectively for the permittivity in vacuum and in the relative permittivity of the semiconductor. ϕ is the electrostatic potential. The driving signals cause a time dependent electric field in the device, therefore displacement current needs also be taken into account.

$$\vec{J_{dis}} = \varepsilon_0 \varepsilon_r \partial_t \vec{E} \tag{4}$$

The diffusion constant D is linked to the mobility by means of the Einstein relation:

$$D_p = \mu_p k_b \frac{T}{q} \tag{5}$$

where T denotes the temperature and k_b the Boltzmann constant.

Local thermal equilibrium needs to be assumed for the Einstein relation to hold. Furthermore the mobility is known to be dependent on the electric field and the charge density for disordered organic semiconducting materials[21]. For ease of use the mobility is kept constant. This constant mobility is the mobility of charge carriers in the accumulation layer of an electronic ratchet device while operated in transistor mode.

Linearization of the equations in this chapter makes it possible to solve them using forward integration in time in MatLab. For each integration step the current densities and charge densities are recalculated. From these new potentials and electrical fields are determined, allowing the currents and charge densities to be calculated again. Etcetera.

Simulations can be done both with and without contacts. The charge carrier densities in the system are in one case a priori determined by the parallel plate capacitor formed by the gate and the accumulation layer and in the other by the injection of the charge carriers via the contacts. In both

cases the simulations have to run for a certain period of time to reach a quasi steady-state before data can be used for comparison with experiments.

For solar ratchet devices described in section 4 recombination currents have to be calculated. Langevin recombination[22] is used for this,

$$R_{n/p,i}^L = \alpha \gamma_L \left(n_i p_i - n_{0,i} p_{0,i} \right). \tag{6}$$

Where γ_L is the Langevin coefficient and α an empirical dimensionless prefactor that is unity for pure Langevin recombination, n_0 and p_0 are the intrinsic carrier densities. This recombination method consist of the free holes and electrons coming close where they can directly recombine.

From simulations in the described program, called DriftKicker, it has been determined by Erik Roeling that for high frequency regimes the influence of diffusion is very small compared to drift[23]. Therefore the much faster FRAT simulation program can be used, FRAT standing for Fast Ratchet Analysis Tool. The representation of the ratchet structure is approximated by simulating it as an RC-circuit. This is valid when the transverse field is much larger than the longitudinal field[12].

The diffusion part of the drift-diffusion equation is being neglected. Poisson's equation for the Coulomb interaction is replaced by:

$$V_i - V_{g,i} = \frac{Q_i}{C_i}. \tag{7}$$

Where Q_i is the charge at cell i, C_i is the capacitance corresponding to that cell and $V_{g,i}$ the gate voltage. Again forward time integration is used to solve alternatingly the drift equation and the continuity equation.

Figure 9 gives a schematic representation of the RC-circuit equivalent to a field effect transistor or ratchet device. The capacitance C_i is chosen differently for finger electrodes and gate contacts, thereby incorporating the placement of finger electrodes halfway in the dielectric. The capacitance of the gate is twice as small as for the finger electrodes. The driving signals are applied by local time-varying signals $V_{g,i}$.
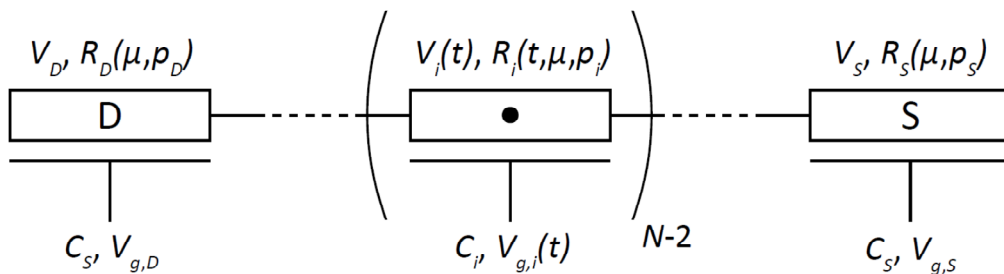
Figure 9 Schematic representation of the RC circuit equivalent to a field effect transistor or ratchet device. S and D are source and drain, V_g is the gate voltage, C_i position dependent capacitance and R_i the resistance of the semiconducting channel which is time, mobility and density dependent. The capacitance C_i is chosen differently for finger electrodes and gate contacts, thereby incorporating the placement of finger electrodes halfway in the dielectric. The driving signals are applied by local time varying signals $V_{g,i}$.[3]

3.6   Fabrication process

3.6.1   (in)-organic electronic ratchet device

Figure 10 schematically shows the fabrication of a ratchet device where the letters will be discussed in the upcoming chapter. The fabrication of ratchet devices starts the same way as making an ordinary FET. In this case the substrate with which is started is a highly boron doped silicon wafer. Besides acting as the substrate it is simultaneously the gate electrode for the device. On top of this substrate 100 nm SiO_2 (Silicon Dioxide) is thermally grown. (Figure 10a)

Next the interdigitated finger electrodes are deposited via a lift-off process. This process consists of applying a negative photo resist using a method called spin-coating. The photo resist is then exposed to ultra violet light through a mask. The non-exposed regions of the photoresist are subsequently washed away, so the negative image of the mask pattern remains. The smallest feature size that can be reached with this method, which is also the typical width of the finger electrodes, is 1 μm. After that, the metals forming the finger electrodes and the contact pads for these electrodes are evaporated. The finger electrodes are made of 20 nm gold between two thin 5 nm layers of titanium. Titanium is used because it attaches better to the SiO_2 and therefore acts as a glue between the gold and the dielectric. The remaining photo resist can be easily removed by washing with acetone. The undercut that is typical for the negative photoresist ensures that the metal layer on the substrate is disconnected from the metal on the resist and can be lift off. (Figure 10b,c,d)

On top of the finger electrodes a second layer of 100 nm of SiO_2 is applied. In this case this is done by Plasma Enhanced Chemical Vapor Deposition (PECVD). It is readily available in the clean room at the TU/e and therefore a logical solution. The source and drain contacts are deposited in the same manner as the finger electrodes. The placement is symmetrical around the finger electrodes. It is important for fingers and contacts to be exactly aligned in order to minimize undesired asymmetries resulting from different pathways of charge carriers to the left and right contacts. The contacts have again an 'adhesive' titanium layer, 10 nm thick with a 40 nm gold layer on top. (Figure 10e,f,g,h)

From this point on, different semiconducting materials require different steps to be taken. Pentacene was shown on top of the electronic ratchet in Figure 7; other materials used are Indium Galium Zinc Oxide (IGZO) an inorganic amorphous semiconductor, Poly 3-HexylThiophene/Phenyl-C61-Butyric acid Methyl ester (P3HT/PCBM) and Poly p-Phenylene Vinylene (PPV) both organic semiconductors. We can divide these materials in two categories. One that needs to be patterned after deposition and materials that require patterning before. In both cases the patterning is needed to avoid undesired electrical pathways between the (contacts to) the finger electrodes and the source and drain contacts. Patterning before deposition is needed for organic materials; the IGZO is patterned after deposition. Patterning beforehand is done by spin-coating a thick layer of negative photo resist which, after structuring, acts as a shadow-mask. Again a negative photo resist is used and patterned with ultra violet photolithography to create the desired undercut. (Figure 10i)

Patterning after the deposition of the semiconducting layer is necessary for IGZO because the process of depositing IGZO is incompatible with the presence of photoresist layer used as shadow mask. In order to be able to use the same structuring pattern the resist needs to be a positive one. In this case the IGZO in the channel region remains covered by a photoresist layer after exposing and removal of the resist. Hence, upon subsequent exposure to acidic acid it is not etched away. Note that this is not shown in Figure 10, where the structuring process for organic materials is shown. The

only steps changing in this case is that after step h the IGZO is deposited and the patterning is done afterwards.

Finally, the deposition of Pentacene is done by first applying a monolayer of HMDS on the exposed SiO_2. On top of that 50 nm of Pentacene is deposited by means of thermal evaporation in high vacuum. P3HT/PCBM and PPV are spin-coated directly on the patterning layer. The approximate thickness of these layers is 100 nm. The patterning layer is 2 μm and therefore disconnects the channel region of each device from the rest of the substrate. IGZO deposition is done at the Holst Research Centre by means of sputtering the IGZO on the finished ratchet device. (Figure 10j)
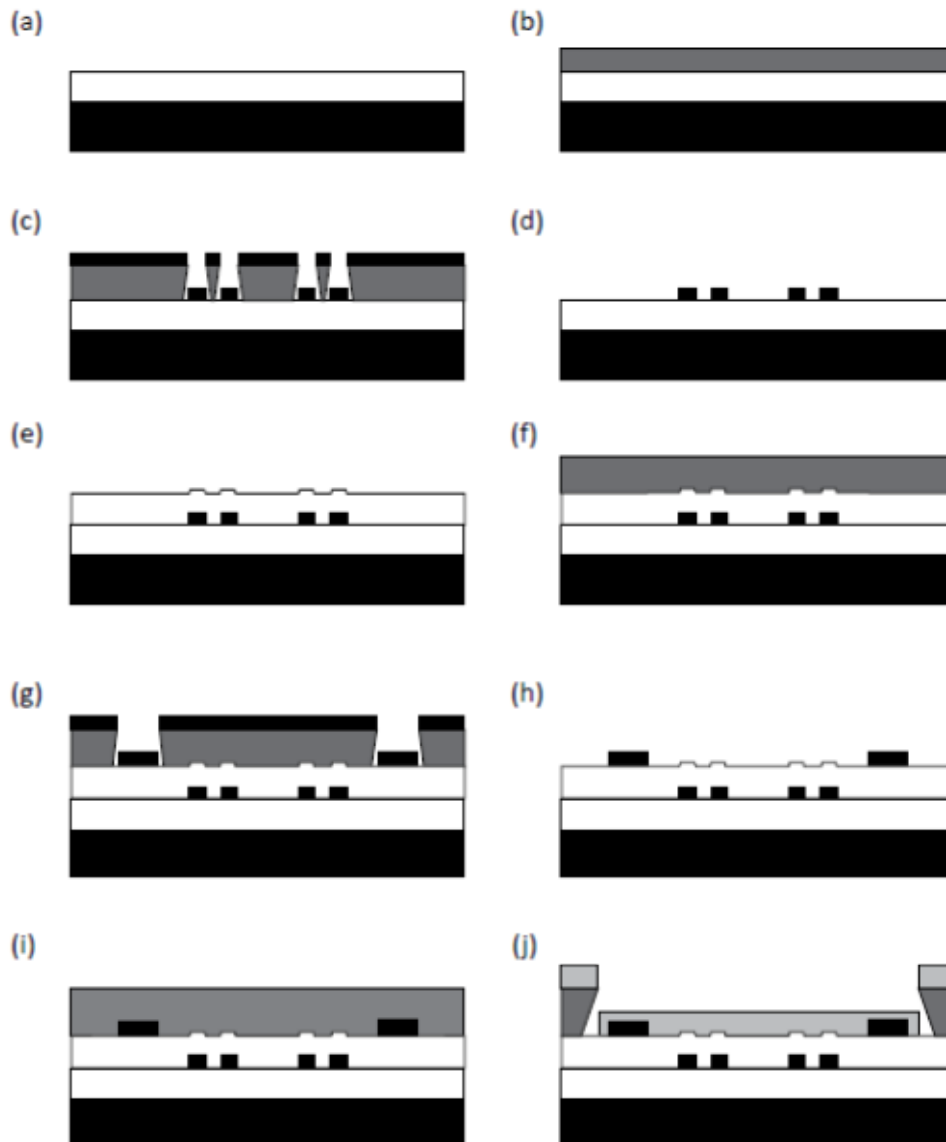
Figure 10 Production of an organic electronic ratchet device. The different production steps shown from a-j are descussed in paragraph 3.6.1. Steps i and j are unique to organic semiconductors. The processing of IGZO ratchet devices is explained in the text.[3]

To expand on the patterning of the semiconductors: This is done because of several reasons. Experiments done by Erik Roeling showed that the leakage current of the devices to the gate becomes comparable to the ratchet currents generated by the device itself[2324]. This can be

understood by the accumulation layer being present on the total wafer, as the gate electrode is common over the total wafer, resulting in a conducting path between the semiconductor and the finger electrodes as well as a high chance of a conducting path to the gate directly over the edges of the wafer. The pathways are decoupled by patterning the devices, negating these problems.

Slight variations can easily be made for these devices, different dielectric thicknesses being the main one. Also the implementation of different semiconducting layers only demands that the patterning layer can withstand the deposition of the material. If not, etching steps as used for IGZO can bring an alternative solution.

3.6.2   Solar ratchet device

The second part of this thesis deals with ratchet solar cells, see section 4. Here, only the fabrication procedure is described. The solar ratchet is of a similar design as the electronic ratchet. With the same design a proof of principle is tried to be made. For the actual device smaller feature sizes are necessary, 100 nm instead of the 1 μm used before. The reason for this will be explained in the second part of the thesis. Here the design is shown and it is explained how we want to produce it. Figure 11 gives a schematic view of the device. A quick glance over the schematic reveals that there is no gate electrode and the finger electrodes are directly placed on a glass substrate. On top of the finger electrodes a layer of SiO_2 is placed. The source and drain contacts are on top of this dielectric. P3HT/PCBM is used as a light harvesting, charge generating semiconductor. The top view also contains resistors which are in the same layer as the finger electrodes.

The production of this device could be done in the same way as the ratchet devices discussed in the previous chapter. However the costs for this would be relatively high. Masks would need to be made for the ultra violet contact photolithography. These masks are fixed when ordered and therefore changes in the design are expensive and slow. The method that is opted for in this case is the use of electron beam lithography. The main advantage is the absence of a physical mask. The features on the devices can be programmed in a drawing program and directly copied to the sample, which gives the option of changing the design in subsequent runs.

Without going into great detail, the principle of electron beam lithography (EBL) is that instead of light an electron beam is used to pattern the photoresist. Subsequent steps are essentially the same as for UV lithography. One can remark that shooting electrons onto a photo-resist on glass leads to charging effects of the substrate, unpredictable deflection of the e-beam and failed devices. This problem can be circumvented by applying a thin layer of gold on top of the photo resist[25].
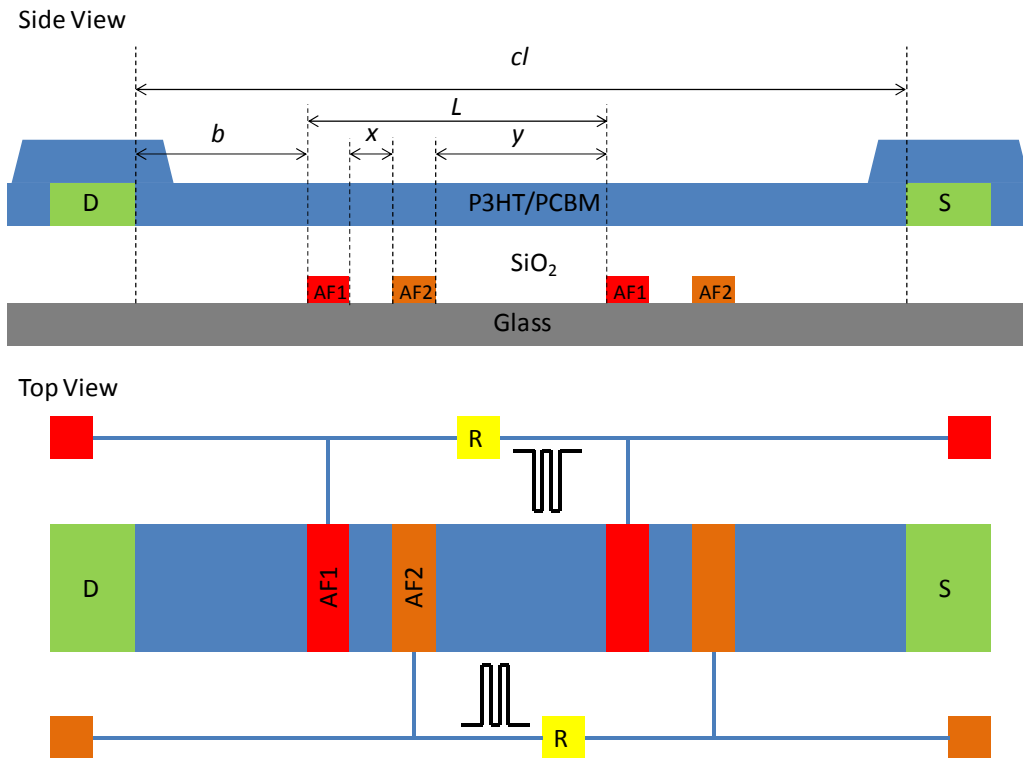
Figure 11 Side and top view of a scaled-down ratchet device which is being optimized for the use as a ratchet solar cell. The nomenclature of Figure 7 is used here as well. Typical feature sizes are here 100 nm. The distance between the source/drain contacts and the first finger pairs is *b*, *x* is the short distance between two fingers, *y* the long spacing between finger pairs, *L* the repeat length and *cl* the channel length. The resistive paths are indicated only in the top view, and consist of a zigzag gold line.

The production of the solar ratchets starts with 2 by 2 cm^2 glass substrates of 400 μm thickness. The glass is cleaned and 200 nm of PMMA is spin-coated on the clean glass. Now a thin layer, ~12 nm, of gold is thermally evaporated on top of this positive photo resist. The EBL can now be used to directly write the design for the finger electrodes along with the resistive paths and the finger contacts onto the PMMA. The thin gold layer can be etched away using a potassium iodine eutectic for 5 seconds, after which the exposed PMMA is removed. Via a liftoff procedure titanium/gold electrodes are deposited. As in the standard ratchet design the titanium is used as an adhesive and the gold for the conduction.

Plasma Enhanced Chemical Vapor Deposition (PECVD) is again used for the deposition of approximately 100 nm of SiO$_2$. Using the same liftoff technique the source and drain contacts are deposited. The device is then ready for the P3HT/PCBM deposition, this time without patterning because this would take too much time and because we first want to look for a proof of principle.

3.7 Experimental setup

Measurements are done inside a high vacuum probe station in which the temperature can be kept constant, typically 300 Kelvin for the majority of experiments. Triaxial probe arms are used to connect an Agilent 81150 dual channel arbitrary waveform generator to the finger electrodes for applying the potentials. The measurements themselves are done with a KE4200-SCS parameter analyzer from Keithley Instruments. This machine is used to source voltage and measure current at the source, drain and gate contacts. Automation of the measurements is done by using Keithley User Library Tool (KULT) and Keithley Interactive Test Environment (KITE) software.

Measurements are done in a specific order. First an IV curve in transistor drive (see Figure 12 and its discussion) is measured to determine the normal transistor characteristics of the device. Normally a sweep from 10 V to -20 V gate voltage at 2 V source-drain potential difference will be sufficient but the range can change depending on the device, wafer and semiconductor. For the actual ratchet measurements the most interesting characteristics of such a transfer curve are the gate voltage for which the threshold voltage is exceeded by 20 V and the mobility of the charge carriers. This particular gate voltage will be the fixed set point of the gate for the rest of the ratchet measurements while the mobility is important to link measurements and simulations.

Next, the absolute offset V_o (Figure 8) needs to be determined for which the ratchet produces most current. With an offset-amplitude sweep of the ratchet this optimal value V_o is sought. In this sweep the offset and amplitude of the driving signal are varied over a selected range of values. The source drain voltage is kept at zero volt bias. For Pentacene these measurements are done at a phase of π and a frequency of 10^6 Hertz, i.e. close to the estimated frequency of maximum current. For IGZO a phase of $\pi/2$ and a frequency of 10^5 Hertz are used. The estimated best values for the frequency used in the offset-amplitude measurements come from extensive testing of samples beforehand and from the currents obtained through simulations.

After the optimal offset and gate voltage are determined the phase-frequency measurement of the ratchet can be performed. The frequency domain over which is measured runs from 10^3 to 10^7 Hz while the phase is swept over a full 360 degrees. Typical results of these three measurements are shown in Figure 12. The exact shape of the latter two types of graphs will be discussed in chapter 0.

In the transistor drive three current curves are seen, red is the gate current which needs to be small in comparison to the currents through the source and the drain. These curves are the same as the ones for the FET shown in Figure 6 which is logical because the driving signal makes the device a FET. The mobility is not shown here but can be extracted from the data, which is automatically done in the KITE software.
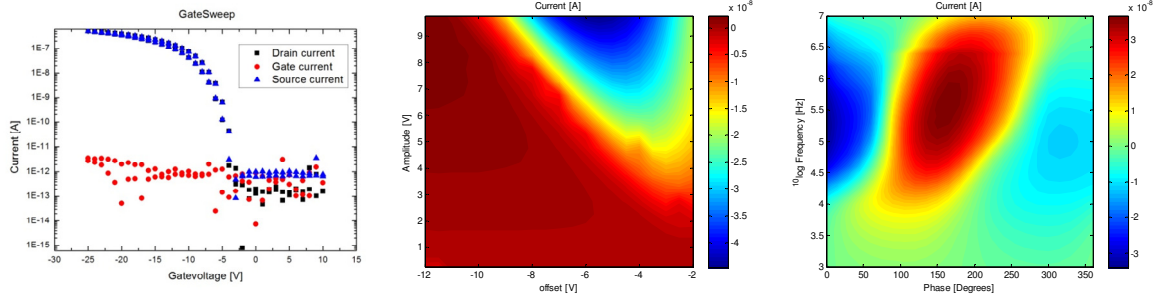
Figure 12 Left panel shows a transfer curve of an organic ratchet device in transistor drive, see Figure 8. It resembles the transfer curve of Figure 6 because the transistor driving signal transforms it in to an organic field effect transistor. The middle and right panel show typical amplitude-offset and phase-frequency measurements.

3.8 Driving mechanisms

The right panel in Figure 12 shows the phase-frequency plot of an organic electronic ratchet. A complex current profile is visible while using a forward driving signal. To understand such a current profile we start with the symmetric driving signal. From this symmetric signal we will go stepwise into the more complex forward and reversed signals. All signals can be found in Figure 8.

The expected current profile in the phase-frequency plots can be found in paragraph 3.4.2 'driving signals'. To iterate, for a symmetric driving signal currents occur at phases other than zero and 180 degrees. Also current reversals as a function of the frequency are expected. The picture for forward and reversed driving signals is more difficult.

The current profile is first investigated with the use of simulations and afterwards compared with measurements. The organic semiconductor used for the experiments is Pentacene.

3.8.1 Simulation organic electronic ratchets

The simulation program used is the FRAT simulation tool explained in, chapter 0 . This simulation program neglects diffusion currents, which is validated when high frequencies with respect to the diffusion are investigated[23]. From literature this is the case when taking Pentacene as the semiconductor material and looking at frequencies ranging between 10^5 and 10^7 Hertz. Simulations are in occasions extended to 10^3 Hertz to cover the same frequency range reached in measurements. Validity of this extension is verified by measurements when necessary.

Simulations were first performed on L1-8Pinf devices. The nomenclature of the ratchets is explained in Figure 7 but is reiterated here. The short distance between fingers is 1µm the long distance is 8µm and there are infinite repetitions of these pairs, i.e. no contacts are present.

Figure 13 shows the simulated current profile when applying a symmetric driving signal to an L1-8Pinf ratchet. The phase difference between the driving signals on the finger electrodes is varied between zero and 360 degrees and the frequencies between 10^5 and 10^7 Hertz.

The current profile has a clover like pattern with four regions where current runs through the device. There is no current at zero and 180 degrees phase. Between 10^5 and 10^6 Hertz the current changes direction at a phase of 180 degrees and as a function of the frequency a current reversal occurs at 2 10^6 Hertz.

For a difference in phase between the two finger electrodes of zero and 180 degrees the simulations calculate zero net current. This is as expected due to the symmetric behavior of the signal and the predictions made in paragraph 3.4.2.

Looking at the low frequencies we see a positive current for φ<180 degrees and negative current for φ>180 degrees. The transport of current is fueled by the charge waves generated by the finger electrode pairs. The phase delay determines the direction of these charge waves. It therefore changes direction when passing φ=180 degrees.

For frequencies over 2 10^6 Hertz we see the same current profile only in the opposite direction. This is because the charge waves form an interference pattern which can change its direction as a function of the frequency. The frequency at which this change in direction occurs can be intuitively understood by looking at the distance between the middle of both finger electrodes, which is 2 µm.

The RC-time of this distance is given by the equation $L^2/V_g.\mu$ [15]. With a channel length of 2 μm, a V_g of 20 Volts and a mobility of 10^{-6} m^2/Vs this results in a corresponding frequency of $5 \cdot 10^6$ Hertz which is close to the value found of $2 \cdot 10^6$ Hertz. This is a very rough estimation of the value of the current reversal. As we will see more factors come into play in determining the current reversal as a function of the frequency of the driving signal. Higher order current reversals are also expected with this explanation and are discussed together with the in-depth study at the end of this chapter.
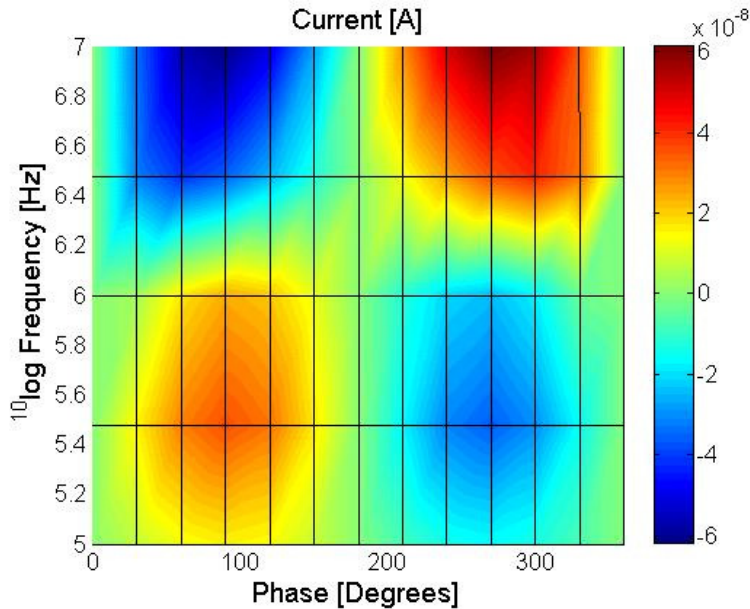

Figure 13 Simulation of a phase-frequency domain of an L1-8Pinf ratchet using a symmetric driving signal with an offset voltage of -7 V an amplitude of 4 V and a gate voltage of -20 V. As can be seen at 0 and 180 degrees phase difference between the finger electrodes the current vanishes. At 90 and 270 degrees phase difference the current becomes maximal solidifying our understanding of the influence of phase on the current passing through an electronic ratchet. The predicted current reversal as a function of frequency is seen at around 2 Mhz.

The Frequency-Phase plot of a symmetrically driven ratchet with current reversals as a function of the phase as well as the frequency is well understood. The difference between the forward/reversed signal and the symmetric signal is the added influence of the difference in offset between finger electrodes as can be seen in Figure 8. These offsets create an extra asymmetry resulting in a non linear superposition of different current contributions.

The offset difference between the finger electrodes is introduced step-wise to be able to investigate the influence of the offset on the current profile of a ratchet exposed to a symmetric driving signal. Figure 14 shows five simulations for which the offsets are chosen to be from left to right, -3 and -11, -6 and -8, -7 and -7, -8 and -6, -11 and -3 volt. Notice that simulation (C) is a ratchet exposed to a symmetric driving signal. (A) and (B) are reversed driving signals, (D) and (E) are forward driving signals.

In panel (B) and (D) we can see the influence of the offset starting to emerge. The four distinct regions in the phase and frequency plot (C) which return current start to merge. In panel (A) and (E) the clover like current profile is transmuted to a profile where the current reversals are determined by the combined influence of the offset, frequency, phase and geometry of the ratchet and its signal.

Looking at Figure 14 panel (E) the maximum current occurs at approximately 180 degrees phase difference between the finger electrodes. From Figure 8 it can be deduced that the forward driving signal at a phase of 180 degrees resembles the on/off ratchet, Figure 2, the most. At this phase difference current reversals are not found as a function of the frequency and the current is in the direction described in Figure 2.

The current profile for φ unequal to 180 degrees is a complex interplay between the different asymmetries mentioned above. The current reversals, now a function of phase as well as frequency, are far more complex and can only be described as the points at which apparently all the contributions to the asymmetry cancel out and no net current is transported.

A second thing to note is the mirror symmetry between (A) and (E), and (B) and (D), to understand this we take another look at the driving signals of the devices with respect to its geometry, Figure 7 and Figure 8.

The device is indistinguishable when inspected from either side because the pairs of finger electrodes are evenly distributed from both sides. The driving signals only differ in offset values and a mirrored phase difference. Whilst keeping the main orientation of the device constant, i.e. source and drain electrodes remain the same, the forward and reversed driving signal result in the same current profile in opposite directions and with mirrored phase characteristics, (A) and (E).

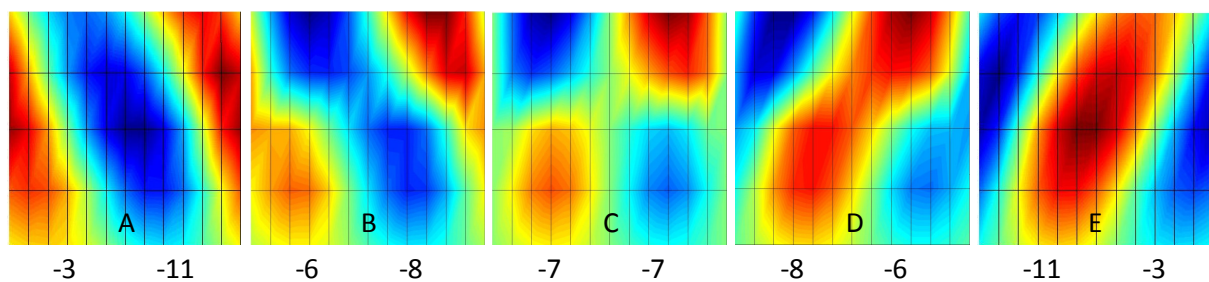| -3 | -11 | -6 | -8 | -7 | -7 | -8 | -6 | -11 | -3 |

Figure 14 Simulations of L1-8Pinf ratchets in which the individual offset voltages of AF1 and AF2 are altered, creating a range of simulations from reversed to forward biasing. The values used for the offsets are respectively -3 and -11, -6 and -8, -7 and -7, -8 and -6, -11 and -3. It shows that the contribution to the current from this offset and from the phase, frequency and geometry are superimposed, resulting in phase frequency plots in which the cloverleaf like current profile disappears and the current reversals are a tilted line trough the phase-frequency domain.

To extrapolate this mirror symmetry extra simulations were done, of which the results are shown in Figure 15. Here, four plots are shown, two with a forward bias signal (A,B) and two with a reverse driving signal (C,D). For each signal the phase is simulated as φ and $-\varphi$, i.e. AF1 lagging behind AF2 and vice versa, creating a picture that is completely inversion symmetric. As can be seen panels (A) and (D) and panels (B) and (C) are identical with only the direction of the current switched.
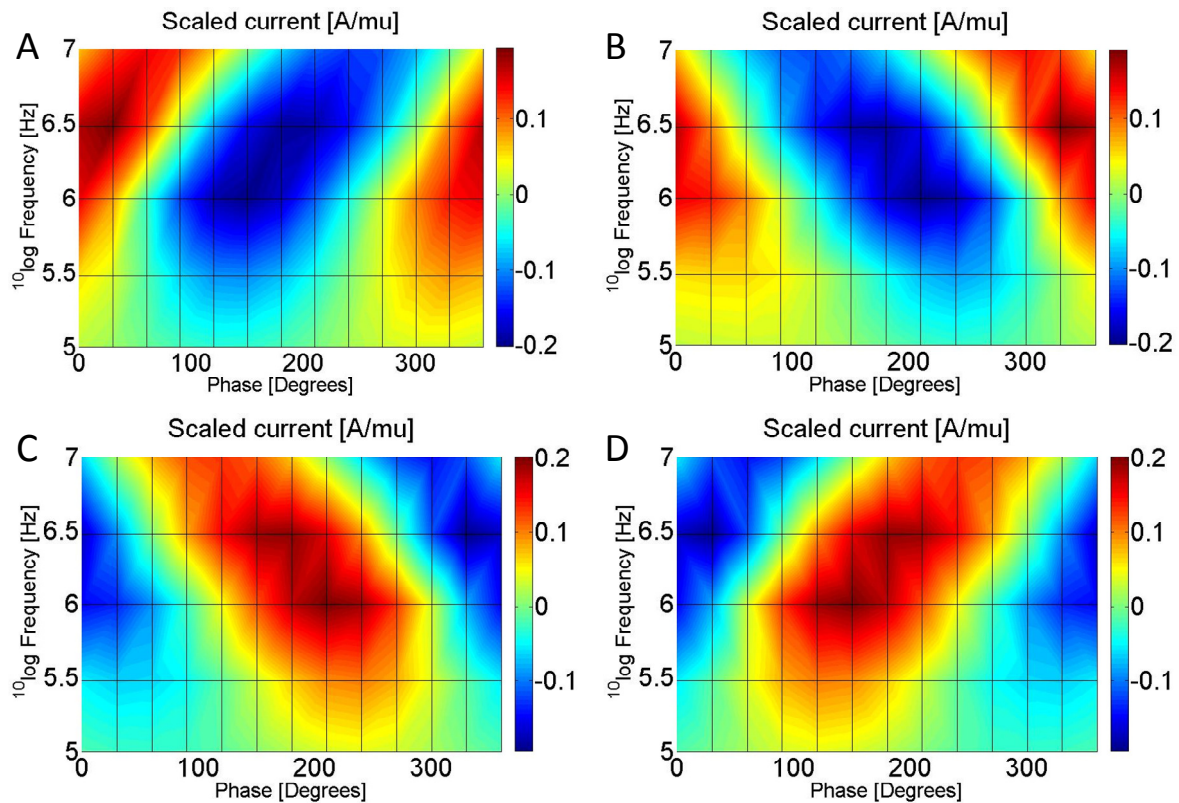
Figure 15 Simulations of the phase-frequency domain of an L1-8Pinf ratchet. Mirror symmetry shown by simulating four driving signals. A and B are subjected to a reverse signal with either AF1 lagging behind AF2 or vice versa, in other words φ =- φ. And C and D are forward signals. A and D as well as B and C are identical with only the directions of the current interchanged.

With the driving signal we can manipulate the current in the device to run in either direction with exactly the same magnitude. If now instead of holes, positive charge carriers, electrons, negative charge carriers, are introduced nothing changes. The mobility is the only factor that changes the current through the device. In other words if the mobility of the holes and electrons would be equal the phase frequency plot is indistinguishable if we drive the system by its inversion symmetric signal.

The dependency of the current reversals on the characteristic length scales as a function of the frequency is explored in Figure 16. Simulations are done with a symmetric driving signal with a phase difference between the finger electrodes of 90 degrees. The frequency is simulated over two orders of magnitude from 100kHz to 10Mhz.

Three cases are explored, first the short distance *x* is varied while the long distance *y* is constant (Figure 7). The top left panel of Figure 16 shows the current as a function of the frequency for four different devices. The current reversals are dependent on the short distance *x* of the ratchet device.

In the bottom left panel the long distance *y* is varied while the short distance *x* is constant. In this case the frequency at which the current reversal occurs is less dependent on the length.

The top right panel shows the current as a function of the frequency for four devices where the ratio between the two lengths is kept the same while the total length is varied. The shift in the frequency at which the current reversal occurs is the most linear in this case.

The frequencies at which the current reversals occur were previously stated to be dependent on the RC-time of the semiconductor, $L^2/V_g \cdot \mu$. The gate voltage and mobility are kept constant for these simulations, therefore the frequencies at which the current reversals occur should abide to a $1/L^2$ trend. The bottom right panel shows a double logarithmic plot of the frequencies at which the current reversals occur with respect to the specific varied length. The solid line in the plot shows a $1/L^2$ trend.

From this plot we can deduce that the change in total length while the ration is kept the same abides this one over L squared trend the best. The first suspected short distance closely resembles it as well. The long distance shows a different behavior in which the current reversals become independent of the length when this length is long enough.

To approach the problem of the length dependency of the frequency at which current reversals occur, the RC-time is a guideline. Because of the nature of the current reversal, a complex interference pattern in the device, the specific length scale which determines this current reversal is hard to determine[15].
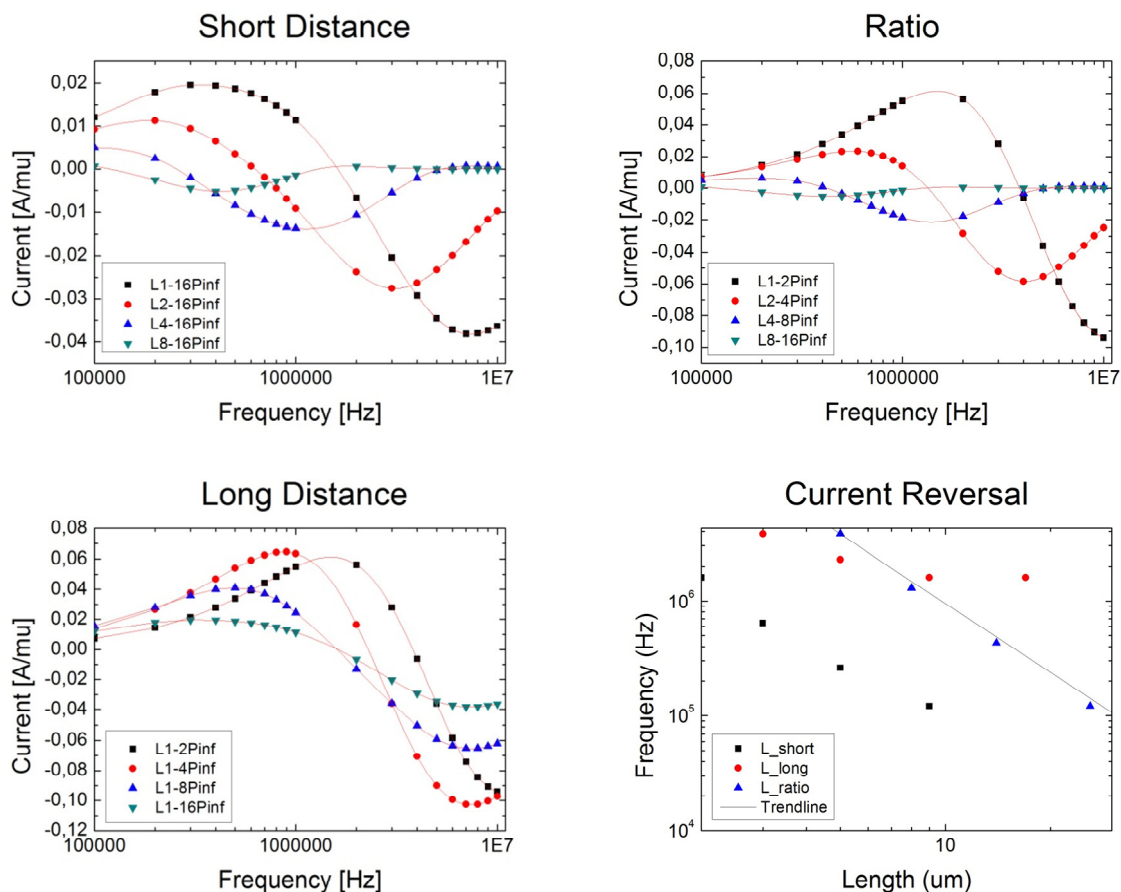

Figure 16 Current reversals of symmetrically biased ratchets at 90 degrees phase difference between the finger electrodes. There is a dependency on both the short and the long distance between the finger electrodes and pair of electrodes. In the top right graph the fraction between these distances is kept the same. The bottom left panel shows the frequency at which the current reversal occurs as a function of the length that is altered. The trendline shows the behavior of c/L^2 with c a typical value at which this trendline corresponds with the behavior of the current reversals as a function of the total length of a repeat unit.

3.8.2   Measurements

Pentacene, which is a high mobility organic semiconducting material, is used as the semiconducting material. It is used because it is extensively investigated and therefore well known. The parameters of the simulations are chosen to be the parameters of Pentacene. Measurements were done to verify the results obtained with simulations for the respective driving signals. For comparison three experimental (left) and three numerical (right) results are plotted in Figure 17.

The simulations and measurements are in qualitative agreement. Starting again with the symmetric driving signal, see Figure 8, the clover like current profile is present in both the simulations and the measurements. The current reversals as a function of phase and as a function of frequency are clearly visible.

For the forward and reversed driving signals the results show that the modeled effect of the superposition of the currents due to the different symmetries is correct. The absolute value of the predicted current is of the same order of magnitude as found in the experiments. For the (upper part of the) frequency regime investigated the drift-only simulations reproduce most, if not all of the physics of the organic electronic ratchet.

Upon further investigation differences between measurements and simulations start to emerge. The differences between simulations and measurements can be caused by two different problems. The first is the incomplete model, no diffusion currents and no local non-equilibrium, used in the simulations and the second is the set of input parameters which are not trivial to obtain.

A difficult to obtain input parameter is the effective gate voltage due to the changing threshold voltage. Bias stress is the cause of this problem. Another difficult parameter is the offset voltage of the finger electrodes. The amplitudes can be used directly but depending on the gate voltage the offset voltage also changes. The more systematic problems lie in the assumption that the mobility is constant while the ratchet is in operation. This is not true due to density dependent charge carrier mobilities[21].

Combining these difficult to obtain parameters with the inherit not simulated effects creates the differences in generated currents between the simulations and the measurements. This is most notable in the symmetric driving signal for low frequencies where the simulations underestimate the current generated by the ratchet.

The simulation for the reverse driving signal is optimized and the ones for the symmetric and forward signals are not. This is due to the process of optimization, which consists of repeatedly performing simulations with slightly changing input parameters. This process is very time consuming. This optimization reduces the influence of the input parameters and consequently shows the best similarity between measurements and simulations. The consequence of this is that the simulation for symmetric and forward driving signals match less with the measurements as the reverse simulation and measurement do.
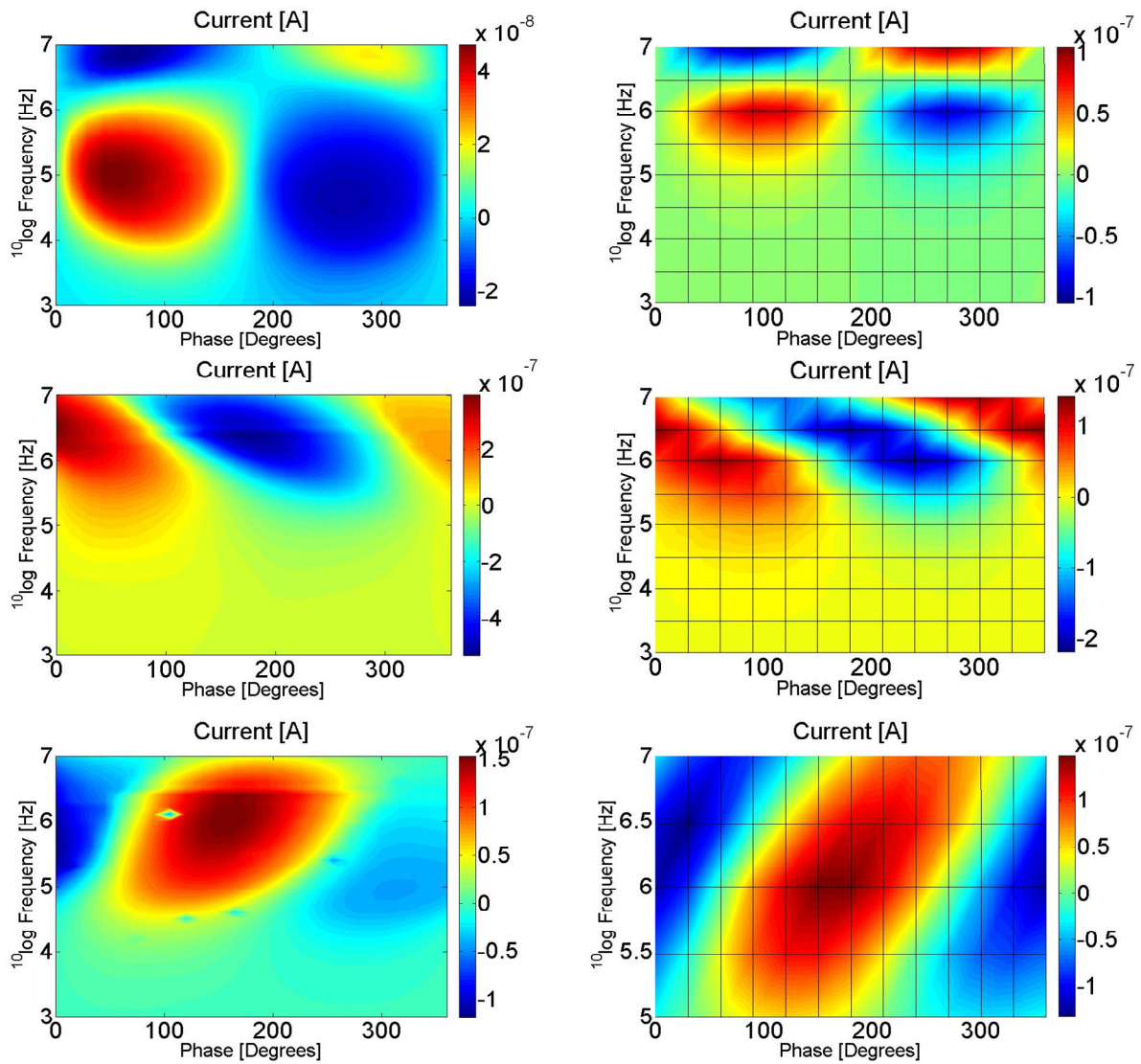
Figure 17 Measurements (left) compared with simulations (right) for symmetric, reversed and forward driving signals (top to bottom). The measurements and simulations are done on L1-8P8 devices in which the gate voltage is surpassing the threshold voltage by 20 V. The offset and amplitude are individually matched for the measurements and simulations. These values are determined in the measurement by the method described in chapter 0.

While discussing the driving signals in paragraph 3.4.2 the on/off ratchet was stated to resemble the flashing ratchet in forward drive at 180 degrees phase difference between the finger electrodes. Inspecting the bottom left plot of Figure 17 we can draw a line at 180 degrees phase and observe the following: from low to high frequencies the current starts out small and increases to a maximum, in this case at 1 MHz, after which it decreases again. No current reversals are found and the description corresponds to the one anticipated for an on/off ratchet, as shown in Figure 2.

Remarkable is the magnitude of the current in the forward and reversed driven ratchets. The offset applied to these ratchets creates a maximum current at 180 degrees phase. However the current at zero degrees is in the opposite direction and is of the same order of magnitude. This again must have to do with the interference pattern created by the finger electrodes. However the exact reason for the magnitude of this current is unknown, even though the simulations show the same values for this current as the measurements.
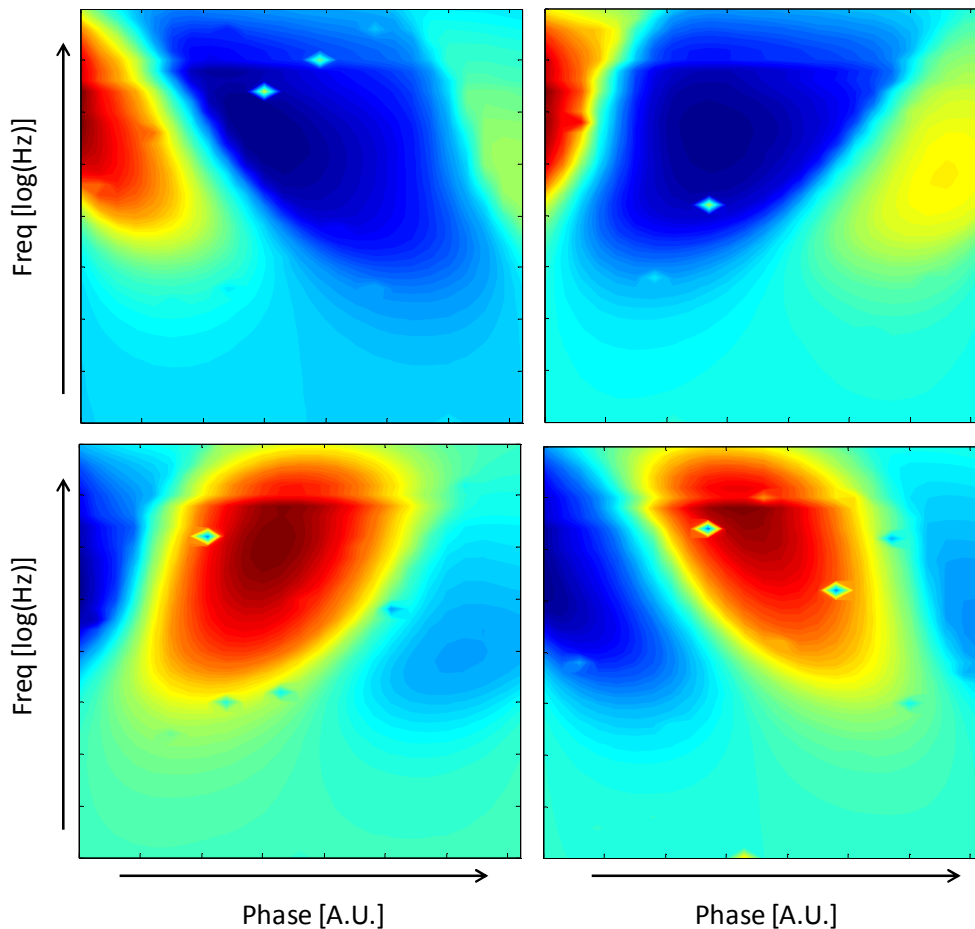
Figure 18 Phase vs. frequency measurements on mirror symmetry of an L1-16P16 system with respect to the driving signal, confirming the results obtained in Figure 15. Two forward and two reversed measurements with in which the phase φ is switched.

Figure 18 shows the mirror symmetry of an L1-16P16 system with respect to the driving signal, confirming the results obtained in Figure 15.

3.8.3   To conclude

A qualitative understanding of (organic) electronic ratchets has been discussed in this chapter. This understanding is divided in three different parts. First we understand the on/off ratchet which holds for the electronic ratchets when driven with a forward or reversed driving signal with a phase φ of 180 degrees.

This no longer holds for phase differences other than 180 degrees: For this case we need a model which includes charge waves and the construction of an interference pattern of these charge waves. These waves and this interference pattern are caused by the driving signals on the finger electrodes which have a phase difference. With this picture current reversals as a function of the phase and frequency can be partially understood, or at least anticipated.

When looking into the exact details of the current profile this also gives problems. The magnitude of the current in the case that the phase is almost zero degrees is remarkable. Simulations confirm these high currents and their directions. A more complex, complete model is needed to describe the exact behavior of the current. However the principles of the on/off ratchet and the interference of charge waves lie at the foundation of this model.

3.9 Scaling properties of (in)-organic electronic ratchets

We claim that the scaling of the generated current for different semiconducting materials as a function of the frequency of the driving signal is only linearly dependent on the mobility of the respective charge carriers. If the mobility of these charge carriers is the only scaling parameters, then combining the results of several semiconducting materials deposited on otherwise identical ratchet devices should be a possibility. The mirror symmetry presented in the previous chapter can be used to combine results of both hole and electron transporting semiconductors.

$$\vec{J_p} = q\mu_p p\vec{E} - qD_p\vec{\nabla}p \qquad (8)$$

Starting from the drift-diffusion equation we see that the current density only depends on the mobility of the charge carriers if the density of these charge carriers is equal for different materials. This follows from Poisson's equation. We already showed that Poisson's equation can be approximated using the equation for a capacitor:

$$\vec{\nabla} \cdot \left(\varepsilon_0 \varepsilon_r \vec{\nabla}\phi\right) = -qp, \qquad (9)$$

$$V_i - V_{g,i} = \frac{Q_i}{C_i}. \qquad (10)$$

These equations are explained in chapter 0 'simulations'. The charge density in the semiconductor is constant when V_i-$V_{g,I}$ is constant, which is taken care of by choosing the gate voltage 20 V over the threshold voltage. Therefore the charge density is independent of the semiconducting material. Simulations are done using the FRAT simulation tool, the diffusion is neglected and the same explanation holds.

Equations 8, 9 and 10 show why the generated current should only scale with the mobility. This scaling now says that the current profile remains the same but is only shifted in frequency with respect to the mobility, i.e. for a semiconductor material with a mobility 100 times higher than pentacene the frequency at which the current profile of Figure 13 is now visible is also a 100 times higher. The current is however also a 100 times larger. This is because for every cycle of the driving signals a certain amount of current is being transported. When the mobility of the charge carriers in the semiconductor and the frequency of the driving signal both increase by a factor of one hundred, the amount of charge carriers transported in one cycle remains equal. Because there are, however, one hundred more cycles per unit of time the current increases by a factor of a hundred.

To correctly compare different semiconducting materials we need to rescale the current and frequency of the measurements. The current can be rescaled by the mobility of the charge carriers in the semiconducting materials. The frequency is scaled by the RC-time of the system. The RC-time is given by $L^2/V_{g}.\mu$ the typical response time of the system. When comparing different materials L^2 and V_g are kept equal. Thereby again scaling the mobility out of the parameters. Now measurements of different semiconductors can be directly compared.

In this project three semiconductors were tested. Pentacene and P3HT/PCBM as hole transporting organic semiconductors and IGZO(Indium Gallium Zinc Oxide) as an electron transporter. The latter is an amorphous inorganic semiconductor.

3.9.1 Simulations

Figure 19 shows the simulation of the current as a function of the phase and frequency of a forward driven electronic ratchet. Seven orders of magnitude in (scaled) frequency are simulated. Therefore the logarithm of the scaled current is taken.

To reduce the simulation time, and at the same time test the FRAT program, the plot is built up from three different simulations. The parameter values used are chosen according to the materials used for the measurements. Combining the three simulations results in an exactly aligned current profile in which the current reversals are visible. To guide the reader the current reversals are marked with dashed white lines.

We scale out the mobility, resulting in overlap of data from high mobility IGZO and pentacene, and low mobility P3HT. When looking at lower frequencies or higher mobilities the current reversals are at approximately 180 and zero degrees phase difference between the signals on the finger electrodes, while for higher frequencies or lower mobilities the already known current reversals with respect to the phase and frequency are visible.
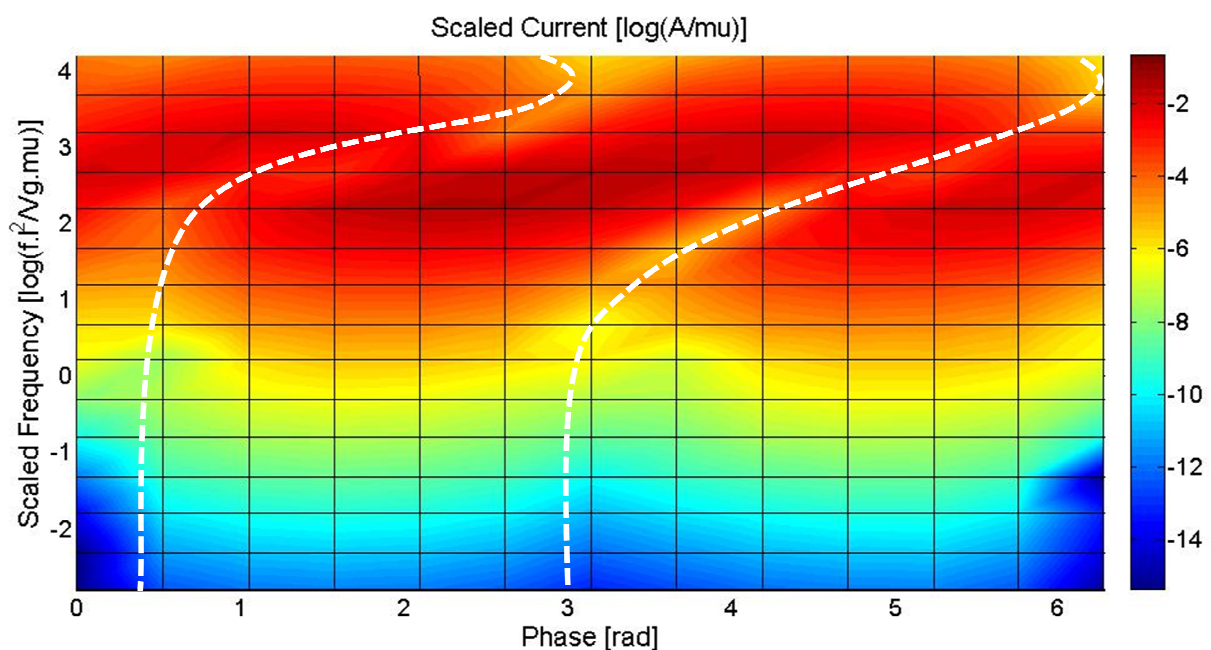

Figure 19 Simulations of the current generated in an L1-8P8 ratchet as a function of phase and (over 7 orders of magnitude in) frequency. The system simulated is similar to the device used in the experiments. The white lines indicate the current reversals in this system. Due to the scaling, data form low mobility semiconductors appear on the high part of the frequency axis and vice versa.

3.9.2 Measurements

As stated before the three materials on which these simulations are based are P3HT/PCBM and Pentacene as hole transporting semiconductors and IGZO as an electron transporting semiconductor. The measurements done are shown on the left panels in Figure 20.

The measurements shown in Figure 20 are chosen because of the quality of the data without regards for the specific direction in which the driving signal is facing. With the system being inversely symmetric it would give the exact same results for the opposite driving direction, if rescaled properly.

The result of measurements for pentacene have already been shown in the paragraph 3.8.2, and is measurement (C). The measurement for P3HT/PCBM is measurement (A). The current profile is shifted in frequency resulting from the fact that the mobility of the material is decreased by a factor of 10. The difference in the direction of the current is due to the fact that it is measured with a reversed driving signal with the phase lag being the inverse as well.

(E) shows the measurement for IGZO. Current is visible for high driving frequencies, this current can be compared to the current generated by the symmetric Pentacene measurements, they correspond with the bottom two 'leafs' of the clover-like current profile, shown in Figure 13. The magnitude and directions of the current in the lower frequencies are unexpected which will be discussed later on.

The fact that IGZO is an electron transporting semiconductor, does not forbid comparison with the hole transporting materials. Again due to the inversion symmetry of the driving signal and the identical but mirrored response, the results can be rescaled for direct comparison.

The simulation results are shown on the right in Figure 20, next to the experimental results. Making use of the inversion symmetry of the system these simulations are all done using the same driving signal, only altering the mobilities for the different materials.
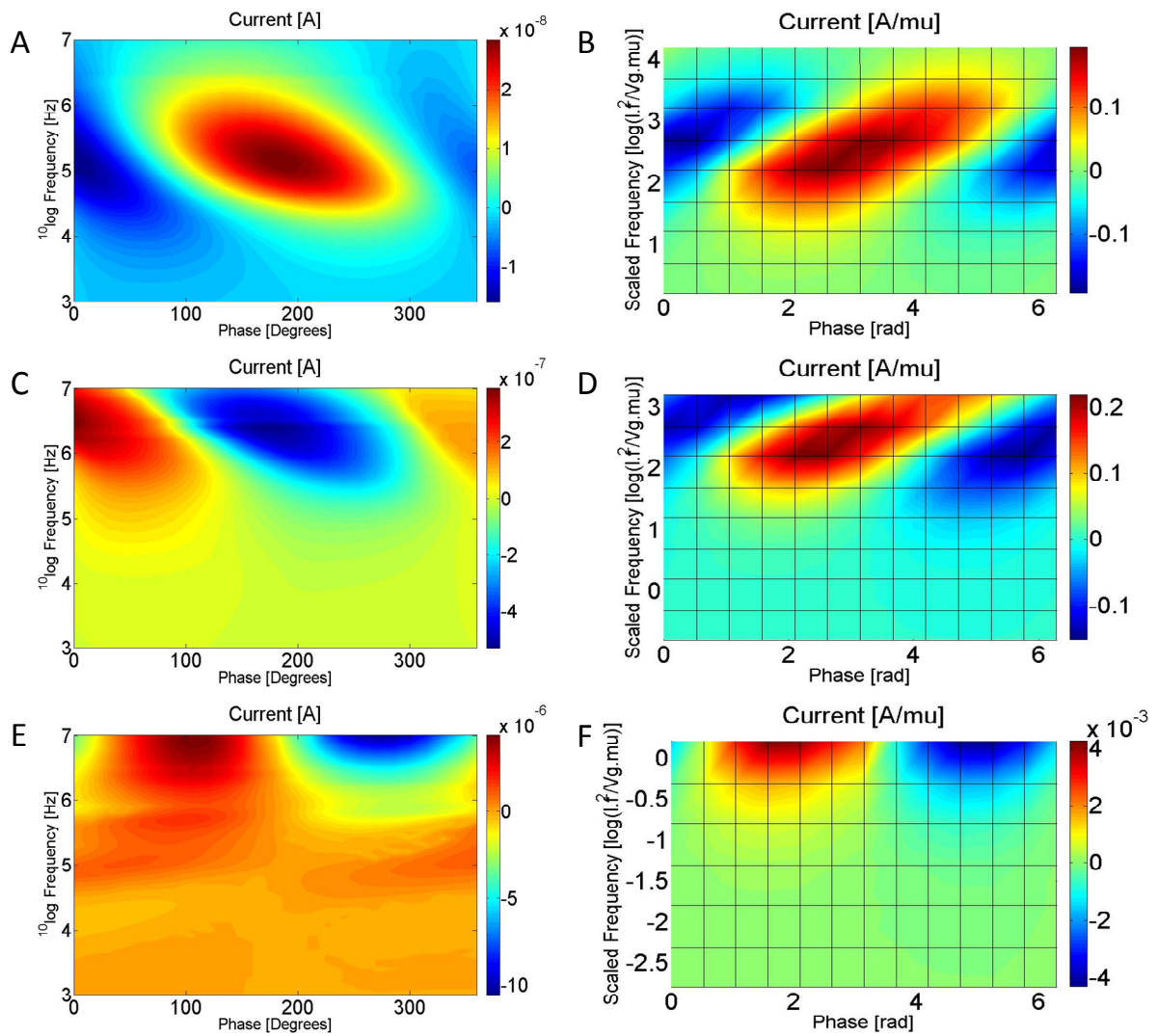
Figure 20 (A), (C) and (E) are phase frequency measurements on respectively P3HT/PCBM, Pentacene and IGZO with the corresponding simulations done for the combined plot of simulations in Figure 19. As can be observed, the direction of the current in (A) and (C) does not match those of (B) and (D). Due to the inversion symmetry of the system this does not matter. The phase, current and frequency in the simulations is chosen as the scaled values which are explained in the text.

Combination of the simulations gives the results already shown in Figure 19. Combination of the measurements in scaled plots is shown in Figure 21 and Figure 22. Again logarithmic current plots are used to combine the scaled currents which range over multiple orders of magnitude.

Comparing Figure 19 and Figure 21 shows the strength and simplicity of the drift-only model used in the simulations . The white lines are again used to indicate the current reversals. The locations for these are the same as for the ones simulated. The simulations are optimized in terms of the used input parameters to achieve this result.

For high frequencies the magnitude of the current matches for measurements and simulations. In the two figures the color schemes in which the current is shown is kept the same, therefore the colors can be directly compared between the two figures.

Low frequencies show currents which are remarkably higher than expected from the simulations. This is discussed in the next chapter.

For three different materials, with both hole and electron charge carriers, measured with different driving signals the scaled picture matches almost perfectly with the simulations. The scaling of the frequency with the RC time causes the low mobility materials to be in the top of the figure and the high mobility materials in the bottom. P3HT/PCBM is in the top with Pentacene in the middle and IGZO in the bottom of the combined phase-frequency plot.
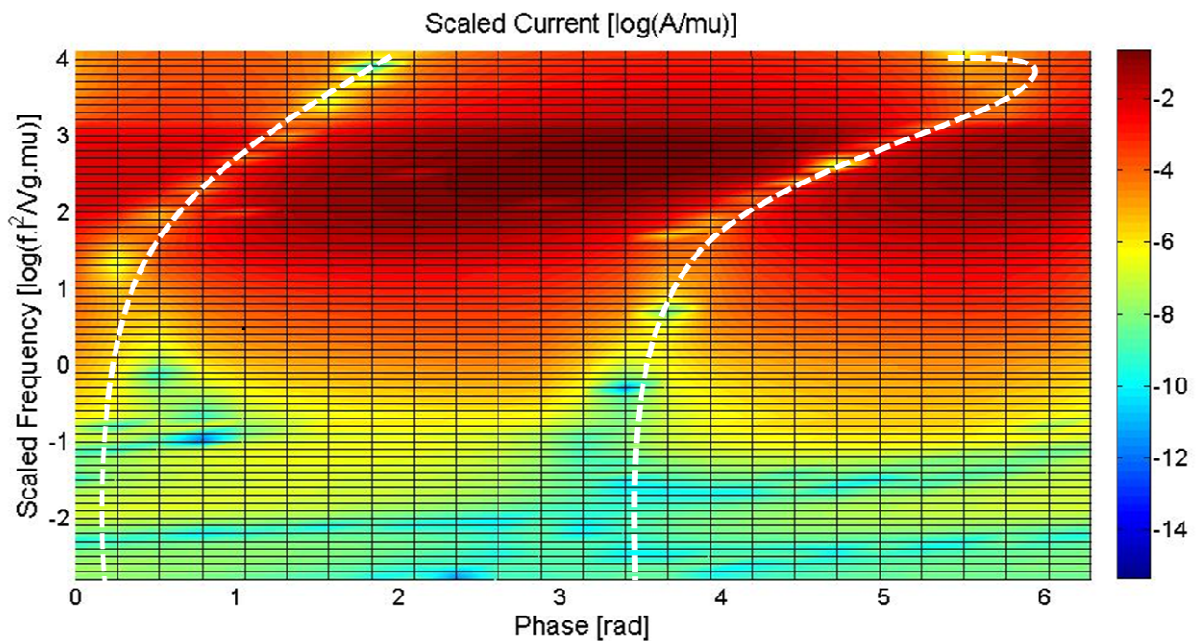

Figure 21 Measurements of the current generated in an L1-8P8 ratchet as a function of phase and (over 7 orders of magnitude in) frequency. Obtained from the three different materials shown in Figure 20 for which the current is scaled with the mobility and the frequency is scaled with the RC-time. From the white dashed lines we see the same current reversals as can be seen from the performed simulations. This result is obtained from two hole carriers and one electron carrier semiconducting material.

Simulations are limited in the time that it takes to calculate them while measurement are limited by the range of the measurement equipment and the physical limitations of the devices. In this case the range of the measurements is larger than the range of the simulations, most notable for the lower frequencies. Therefore Figure 22 shows a plot with the full rescaled frequency range. Two extra current reversals are clearly visible and shown with two extra white dashed lines. These current reversals are found in the measurements for the IGZO material. Simulations should pick up the first of these current reversals, the simulations reach these frequencies, but they are not visible in any simulation.
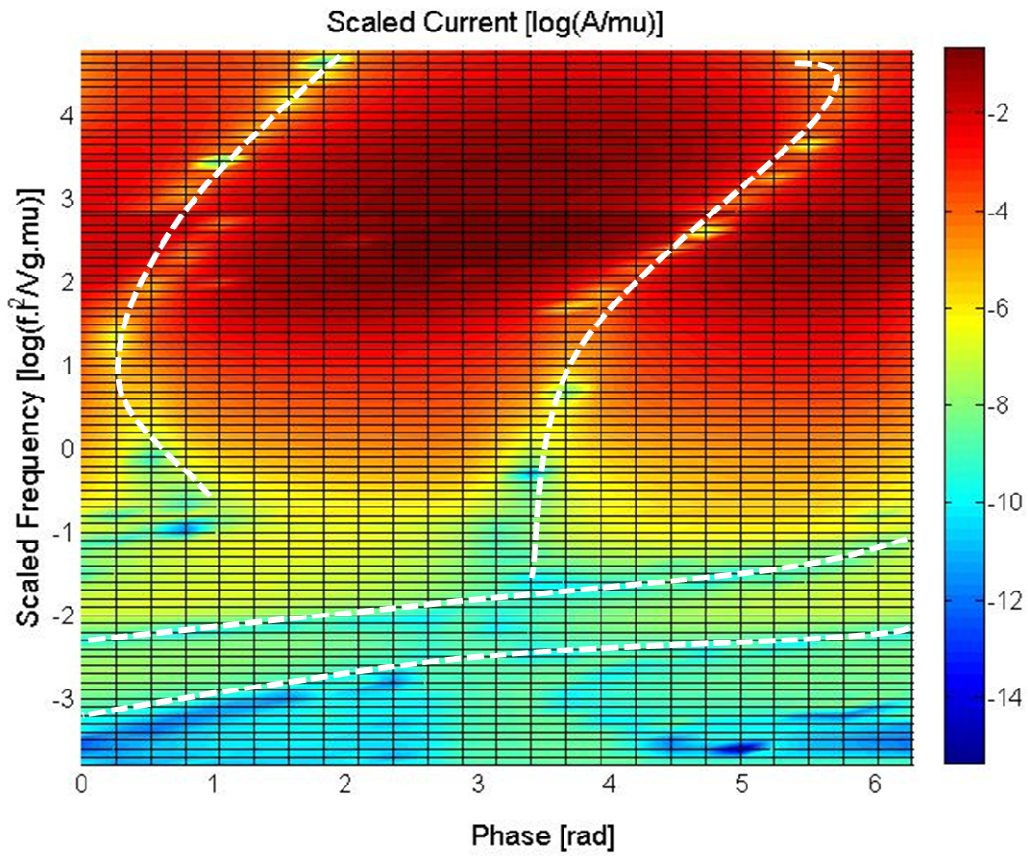
Figure 22 Simulations are limited by their calculation times, the lower frequencies are therefore not reachable. Measurements are limited by the equipment which has a larger reach, these extended measurements are shown here. Very peculiar current reversals can be seen in these low frequencies. This region is measured from the IGZO semiconductor. The middle area is Pentacene and the top area is from measurements on P3HT/PCBM.

3.10 IGZO current reversals

Figure 20 (E) shows the phase-frequency measurements of the current profile of IGZO coated electronic ratchets. Two extra current reversals become apparent for the signals driven with low frequencies. The nature of these current reversals is unknown to us as of now.

To clearly visualize these currents we replot the currents as charge per cycle of the electronic ratchet, i.e. I/f. In Figure 23 this charge per cycle is shown. Up until now all the plots varying the phase and frequency show either the current profile or a scaled current profile of the electronic ratchet. The charge per cycle or CPC of the electronic ratchet is the amount of charges that passes through the device with every full period of the driving signal.

As has been stated before when the mobility and frequency scale in the same manner the current scales by the same amount. The CPC stays equal in this case. With this representation low frequency behavior can be represented much more clearly. The charge per cycle for these extra current reversals is extremely high, two orders of magnitude higher than the charge per cycle generated by Pentacene and P3HT/PCBM at comparable (scaled) frequencies. The values are also much bigger than the CPC generated by the higher frequency signals of IGZO, thereby ruling out the possibility of it being equipment dependent. If that would be the case the current reversals would also be visible for Pentacene and P3HT/PCBM.

The explanation for these current reversals and magnitude of currents cannot be found in the simulations, as they are not present here. The list of tested modifications made to the FRAT simulation program, and which give no notable changes in output, includes contact barriers, misalignment of finger electrodes and asymmetric potentials on finger electrodes.

The IGZO used for these measurements has a mobility of 10^{-3} m^2/Vs. Combining this observation with the low frequencies at which these reversals occur the conclusion can be made that diffusion can no longer be neglected in the simulations. When comparing the mobility of IGZO to the mobility of pentacene and scale the frequency it corresponds to frequencies of 1 to 100 Hertz. For these frequencies the approximation of not including diffusion currents are not valid. This makes the bottom part of the combined simulation unreliable.
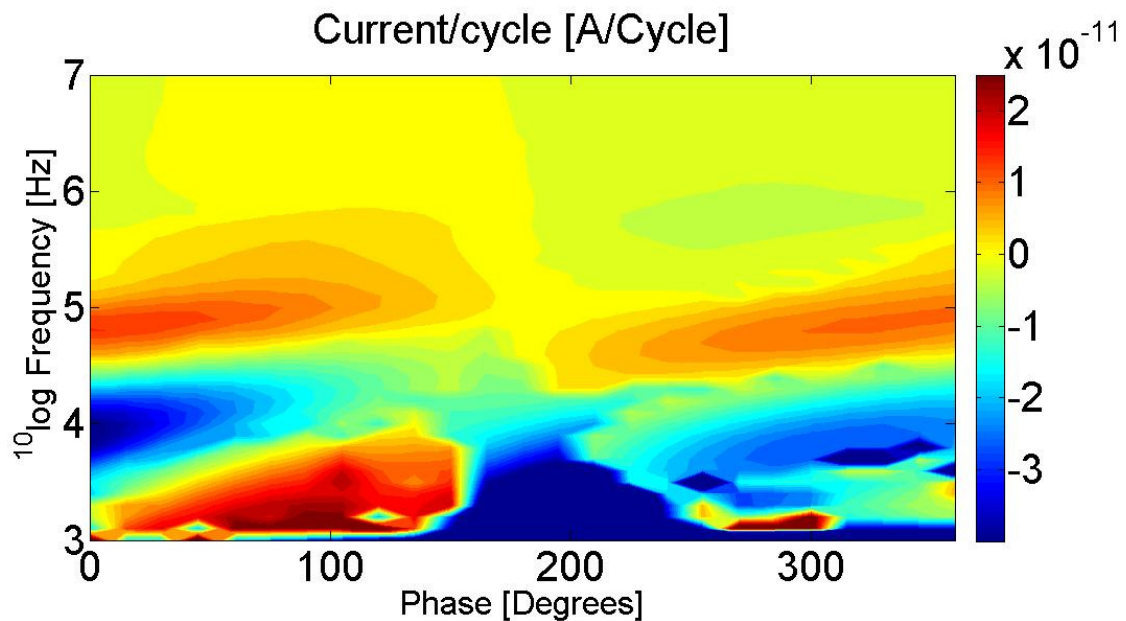
Figure 23 Charge per cycle plot of an IGZO measurement clearly depicting the unusual behavior in the low frequency regime. The region between 100kHz and 10MHz shows the expected behavior in which the normal current reversal at around 20 and 200 degrees are visible. However the charge per cycle is very high for the lower frequencies.

Measurements can learn us multiple things in this case. Figure 24 and Figure 25 Shows two properties of these current reversals occurring at low frequencies. Logarithmic plots of the current in the phase-frequency domain of L1-8Px devices is shown. A large number of finger electrode pairs seems to be essential for the formation of these current reversals.

The five plots give measurements of devices with increasing number of finger pairs. For 2 finger pairs the current reversals are not visible while for 4 pairs they are starting to show. This builds up until at 16 and 32 repetitions of the finger electrode pairs the current reversals are clearly visible and the maximum magnitude of current is reached. We do not have an explanation why there are more repetitions needed for this phenomenon to occur.
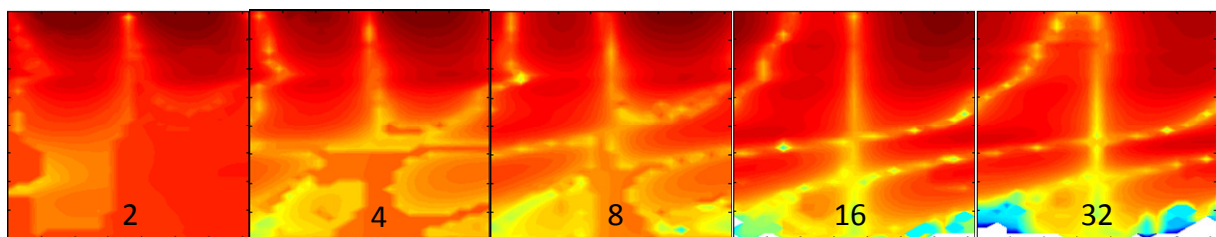

Figure 24 Five logarithmic current measurements with increasing number of finger electrode pairs. L1-8Pz in which z is noted in the plots ranging from 2 to 32. Current reversals are visible as bright yellow lines in between red areas. As can be seen the extra current reversals are not apparent with only two pair of finger electrodes. And becoming visible with 8 finger pairs and sharp in 16 and 32 repetitions.

The next thing to note is that the biasing signal is of no influence to these specific current reversals. As seen before, mirror symmetry is a useful tool to manipulate the results of different semiconducting materials or driving signals for comparison.

The measurements in Figure 25 shows that the current reversals for low frequencies do not change direction while the drift currents do. (Note: this inability to rescale this IGZO current was taken into

account for the combined measurements and simulations. The measurement of the IGZO coated ratchet are used as the default direction therefore upholding the right to use the inversion symmetry in the measurements to combine the results.) The combined evidence excludes drift as the driving force for these currents, diffusion is a more likely candidate as the origin.
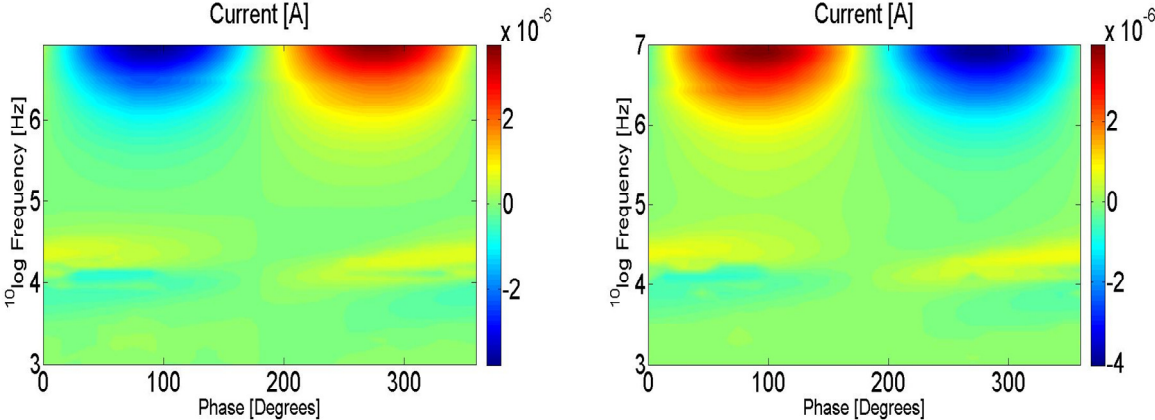

Figure 25 A measured forward and reversely driven electronic ratchet covered with IGZO semiconductor material. As expected the main currents get swapped, red becomes blue and blue becomes red. When looked closer to the current reversals in the lower frequencies these do not alter their direction. Currents are running both times in the same direction. Removing drift currents as an explanation for these currents and its reversals.

4 Organic electronic solar ratchets

4.1 Solar cells

A conventional organic solar cell needs to be understood before looking at an organic electronic solar ratchet. We start from the geometric representation of a solar cell which is shown in Figure 26. A solar cell consists of three parts, a transparent front contact, a photovoltaic material and a back contact. Sunlight goes through the transparent front contact into the photovoltaic material in which it creates holes and electrons. These holes and electrons are transported to the front and back contacts. When the front and back contact are connected in an electronic circuit power can be harvested from this device.
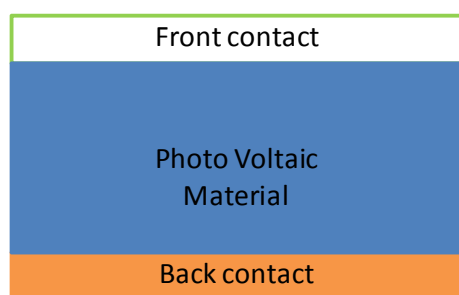

Figure 26 Basic design of a solar cell which consists of two contacts of which at least one should be transparent with in between a photovoltaic material.

Electron and hole creation occurs when the energy of the incoming light is sufficient to transcend the bandgap of the photovoltaic material. This will result in an electron being excited from the HOMO level of the material into the LUMO level, see panel (A) of Figure 27. Because of the Coulomb interaction between electrons and holes, this excited electron forms a bound pair with the hole left behind in the HOMO level, an exciton.
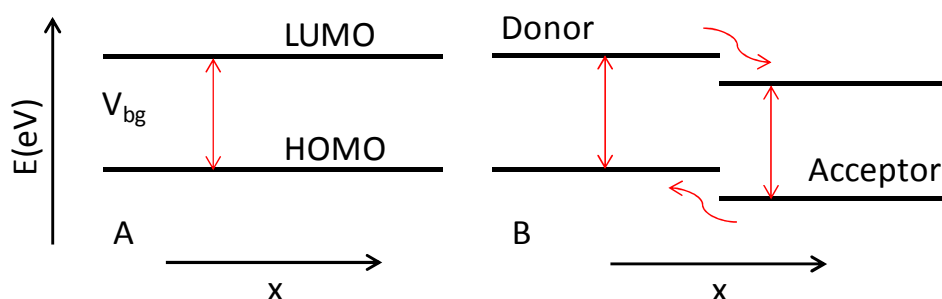

Figure 27 Panel A visualizes the bandgap of a semiconducting material with LUMO the lowest unoccupied molecular orbit and HOMO the highest occupied molecular orbital. Panel B shows a photovoltaic material consisting of a Donor and an Acceptor material. The straight red arrows show the creation of an exciton which dissociates trough the transfer of holes and electrons to most favorable energy levels.

To generate current in the solar cell the electrons and holes need to be transported to the contacts. For that to happen the exciton created by the sunlight needs to be dissociated so the charge carriers are free. In a single organic photovoltaic material this is an inefficient process, the binding energy of ~0.5 eV of the exciton is too large to thermally overcome. The solution is adding an extra material in the form of an acceptor. Figure 27 (B) shows the band diagram for the situation in which there are two materials. An exciton is created in the donor material; at an interface between the two materials

this exciton can dissociate by electron transfer to the acceptor because the total energy for the entire system is lower with the electron on the acceptor. Vice versa for the excitons created in the acceptor, the hole can be transferred to the donor because of a lower total energy.

The electrons and holes are now dissociated, and may, for the present discussion, be considered to be free to move out of the semiconductor. An electric field over the device is needed to extract charge carriers from the bulk to the contacts. This field is obtained by choosing different materials for the front and the back contact. The difference lies in the work function of these contacts. The work function χ is the energy needed to excite an electron from the material to the vacuum. The difference in work function between the two contacts is the build in voltage, V_{bi}. The left panel of Figure 28 sketches the situation described here. The left and right contacts are the cathode and anode and their respective work functions are shown by the energy difference to the vacuum level.
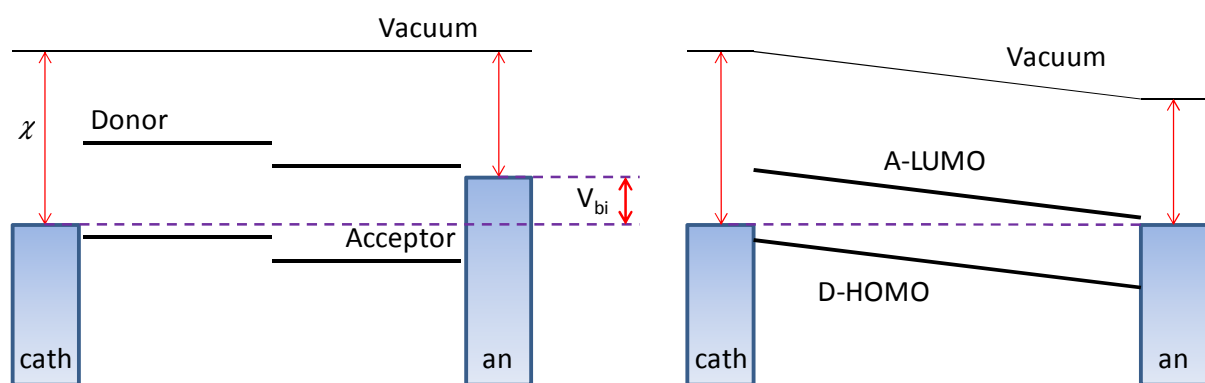

Figure 28 The left panel show the energy levels of the different materials of a solar cell. Here the build in voltage V_{bi} and the work function χ are highlighted. The right panel visualizes what happens when the cathode and anode of a solar cell are shorted which creates an electric field over the photovoltaic material. Note that only the acceptor LUMO and the donor HOMO level are shown because the charge carriers are transported on these molecular orbitals.

The right panel of Figure 28 shows the result at short circuit between the cathode and anode. The energy levels of these contacts need to align to reach equilibrium, which creates an electric field over the semiconductor. This electric field transports the electrons and holes out of the device. Note that the OPV(Organic PhotoVoltaic) material consisting of a donor and an acceptor material is treated as an effective semiconductor with a bandgap that is given by the energy levels of the LUMO of the acceptor and the HOMO of the donor. These are the respective transport bands for the electrons and holes in the OPV. The exact behavior of the energy levels at the contacts is not shown here.

The voltage for which the device returns no current is called the open circuit voltage V_{oc}. It is determined by the energy difference of the quasi Fermi level of the electrons and the holes which are located in the LUMO of the acceptor and the HOMO of the donor. This V_{oc} is typically smaller than the built in voltage of the device.

As we have seen the dissociation of photocreated excitons occurs at the interface of donor and acceptor materials. To maximize the efficiency of dissociations the interfacial area needs to be maximized. A so called bulk hetero junction is created to obtain this, see Figure 29, meaning nothing more than a maximization of the interface while each material is still in direct contact with respectively the anode or the cathode[26272829303]. The hetero junction is created by depositing a blend of the donor and acceptor material in a common solvent on the substrate whereupon phase separation during drying creates the desired morphology.
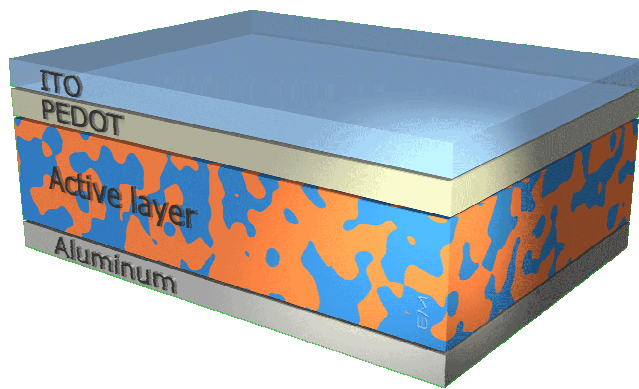
Figure 29 Bulk hetero junction in the active layer of an organic solar cell.[31]

4.2 Tandem solar cells

The energy (or wavelength) of light that is needed to form an exciton is dependent on the bandgap of the photovoltaic material. Large bandgap materials correspond with light with a short wavelength. For materials with a small bandgap light with longer wavelengths can also excite an electron-hole pair. The V_{oc} of the blue(short wavelength) absorbing OPVs is typically larger than the V_{oc} of the red (long wavelength) absorbing materials. The excess energy of the incoming light, i.e. photon energy above the bandgap, is lost in the device trough thermal relaxation of the created electron and hole to the lowest available energy states. Combining these two insights led to the development of tandem solar cells.
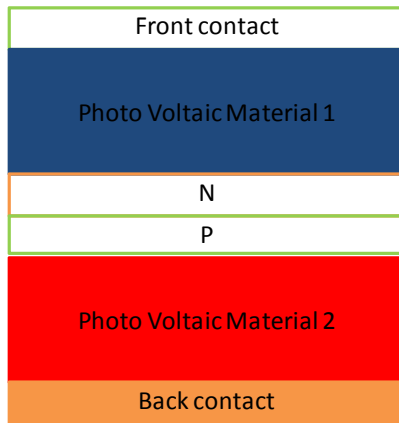

Figure 30 Tandem solar cell which contains two photovoltaic materials with different bandgaps to utilize more light of the spectrum of the sun. Between the two layers an PN-junction is placed which recombines the charge carriers generated in the two photovoltaic materials to create a path for the current.

Figure 30 shows a schematic drawing of a tandem solar cell. A high bandgap 'blue' material is used as material 1. Energetically high, short wavelengths are absorbed while the long wavelengths pass through this material. For material 2 a small bandgap 'red' material is used. In this way more light is efficiently absorbed by the device, i.e. with minimal thermalization loss[32].

To extract current out of this device the photovoltaic materials cannot be in direct contact. Ideally the combined V_{oc} of both subcells is obtained from the tandem solar cell. This is achieved by adding a contact or recombination layers between the two active regions. In Figure 30 this is done by introducing highly doped p- and n-type organic semiconductors stacked on top of each other, i.e. a pn-junction[33], as the contact or recombination layer. Figure 31 shows the band-diagram, it shows that the V_{oc} of both subcells contribute to the combined open circuit voltage of the tandem device.
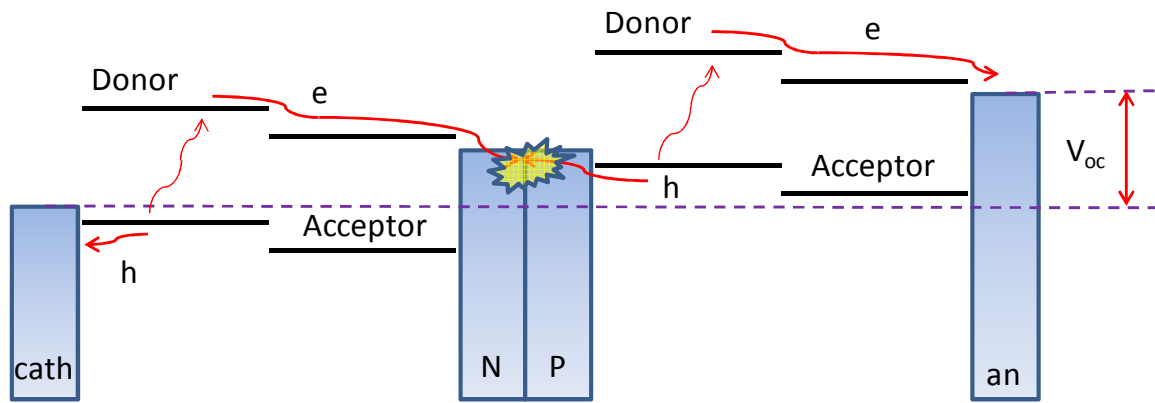
Figure 31 A band diagram of a tandem solar cell which shows the generation of charge carriers, the recombination zone in the PN-junction and the addition of the V_{oc} of the two subcells.

In the device the electrons and holes quickly recombine at the pn-junction. Ideally the quasi Fermi level therefore remains constant over this junction. Figure 31 and Figure 32 show how this recombination takes place. Due to the band bending in the highly doped regions the electrons from the acceptor come spatially sufficiently close to the holes from the donor to recombine.

Because of this recombination zone the current generated in both subcells will be forced to be equal. Simply put, for every acceptor electron there must be a donor hole. If this carrier generation is not in balance the excess charge carriers will accumulate at the doped regions until steady state is recovered and balance between the generation rates is enforced.
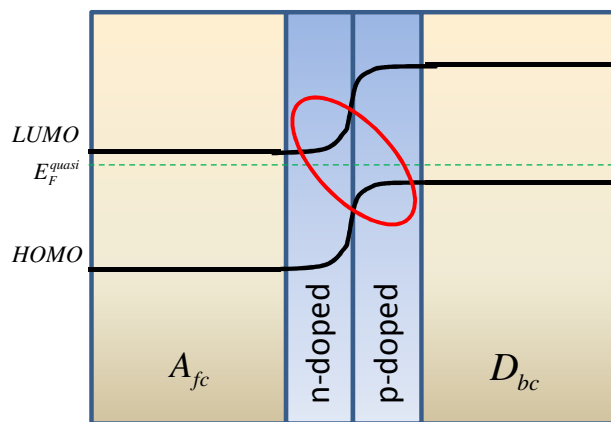

Figure 32 Closer look at the band diagram of the PN-junction where the red encircled area is the zone where the recombination takes places with A_{fc} the acceptor material of the front cell and D_{bc} the donor of the back cell. The green dashed line shows the quasi Fermi level of the electrons and holes in the system.

4.3 Organic electronic solar ratchets

The tandem solar cell can also be used in a peculiar way. In that case the photovoltaic materials are kept the same throughout the device and the layers are made very thin. A stack of several active layers can be made with pn-junctions in between. Instead of what happens in a traditional tandem cell the same part of the light spectrum is absorbed by every part of the solar cell. However, the effect of adding the V_{oc} of every sub-cell remains the same. This will result in a device with a lower current output but with a higher V_{oc}. The power output of the device is the current times the voltage and therefore the intrinsic efficiency remains the same.

The organic electronic solar ratchet is a device that in essence tries to achieve the same as the tandem solar cell described in the previous chapter. We are interested in this device because it will reduce resistive losses of the device due to stacking of V_{oc} and the reduced dissipation due to the lower current densities which reduce resistive losses, ideally resulting in higher efficiencies. The design of this solar ratchet is shown in Figure 33. The design differs substantially from both the solar cells and the by now 'traditional' organic electronic ratchets. While discussing the new device, comparisons to both the ratchet and the solar cell will be made.

From the side view of the solar ratchet we can see that there is no gate electrode; it is replaced by a glass surface. Solar cells generate charge carriers in the organic photovoltaic layer, a gate electrode is not needed to induce these carriers. Furthermore an equipotential surface formed by a metal gate would hinder the buildup of a large V_{oc}, therefore an isolator is used as a substrate. The contacts are called the source and the drain, remnant to the field effect transistor. They are however nothing else than the contacts, cathode and anode, used for solar cells.

The orientation of the device is different from normal solar cells, it is a 'lateral' device. The advantage of this is that the light can reach every part of the OPV material with the same intensity and that everywhere the same amount of current is being generated. Therefore there is no theoretical boundary to the length of the device and subsequently the open circuit voltage. A disadvantage of this approach is that the charge carriers generated by absorption in the recombination zones are lost and thereby reduce the efficiency of the device.
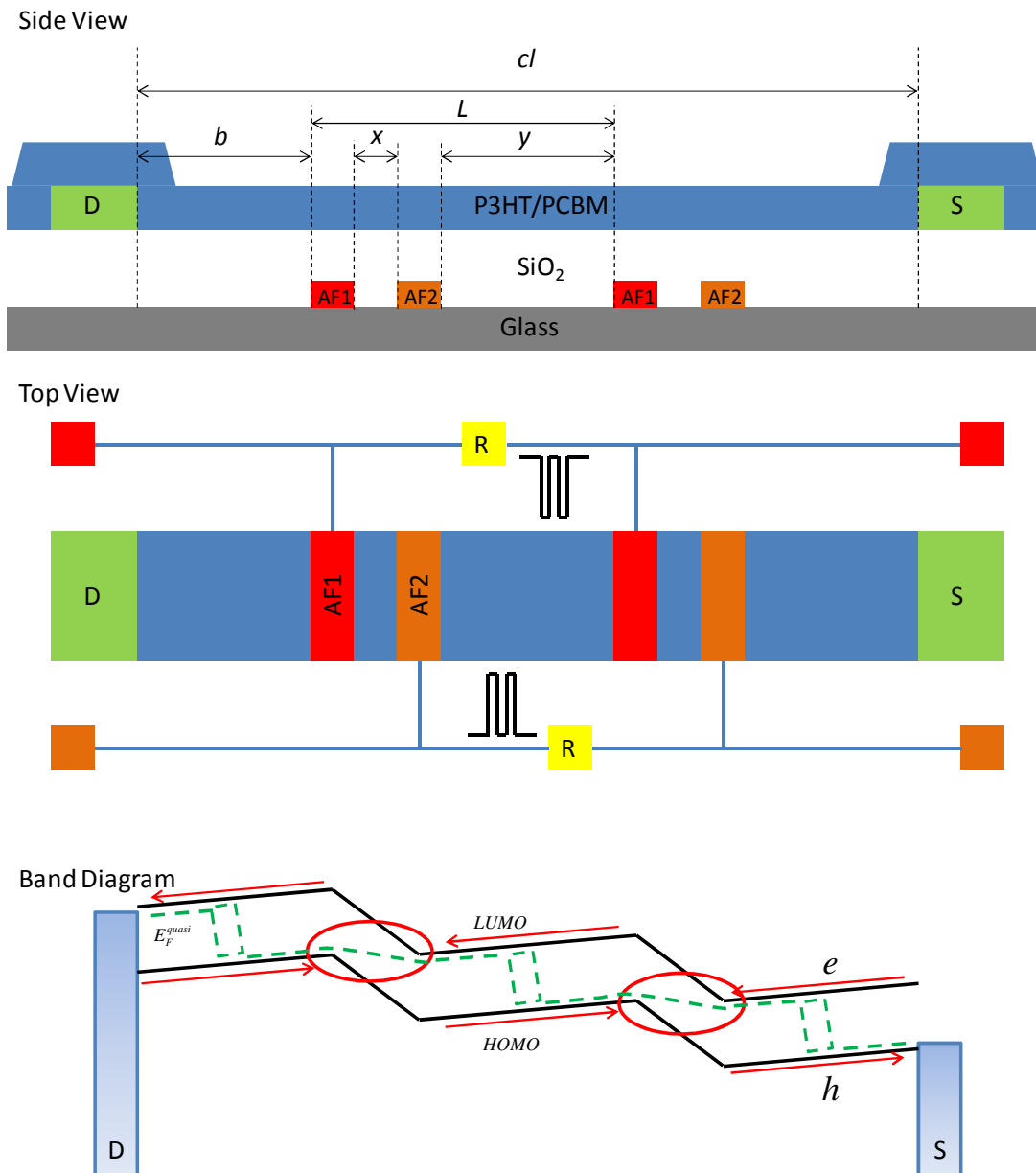
Figure 33 Organic electronic solar ratchet with the side and top view of the device and the band diagram in the last panel. The nomenclature of the parameters in the side view are the same as in Figure 7. In addition the top view shows the resistive paths between the finger electrodes. The band diagram visualizes the recombination zones (red circles) and the direction of the movement of the charge carriers (red arrows). The green dashed lines resemble the quasi Fermi level.

The finger electrodes AF1 and AF2 shown in both the top and side view of the device are also present in the ratchet discussed in the previous section. Comparing them with the ratchet, the finger electrodes are still used to enforce an asymmetric potential profile in the semiconducting channel. The band diagram in Figure 33 shows the influence of the finger electrodes. Looking at it from the point of a solar cell these finger electrodes create the recombination zones (encircled in red). The band bending is not done by doping, as is the case for the pn-junction, but by changing the potential of the region with the finger electrodes. To spatially separate the electrodes a minimal distance of 100 nm is left in the design. The finger electrodes also have a width of 100 nm. The feature sizes should in essence be as small as possible; to make the manufacturing however not impossible a size of 100 nm is chosen.

The areas in between the finger electrode pairs are now the 'subcells' of the tandem solar cell. The lengths of sections b and y are equal because of the recombination zones at the short distance x between AF1 and AF2. The number of charge carriers coming from either side need to be equal to prevent accumulation of excess charges.

The length of these subcells is in the order of several hundred nanometers. The potential difference between the subcells can never be larger than V_{oc} else no current will be generated. Moreover, the field over the subcell has to be as large as possible to yield the maximum current. The internal quantum efficiency, the fraction of charge carriers coming out of the subcell per absorbed photon, is dependent on the potential over the subcell. A tradeoff between this quantum efficiency and the 'relative lengths', between recombination zones and subcell sizes, needs to be made to determine the optimal length of each subcell.

The resistive paths shown in the top view of Figure 33 are needed to tune the relative potentials on the pairs of finger electrodes. The potential created needs to be evenly distributed over the device to create the same band structure as in a tandem solar cell. As can be seen in the band diagram of Figure 33 the energy of the recombination region lies in between the energy of the cathode and anode. When we increase the number of subcells each recombination region needs a different energy and thereby the finger electrodes should be at different potentials. To exclude the need to connect each finger electrode individually resistances are placed in between. If now both contacts of AF 1 (red) will be connected a bias can be chosen such that the distribution of the potentials over the finger electrodes of AF1 is evenly distribute to create the same band structure as in the pn-junction of a tandem solar cell.

4.4   Solar ratchet simulations

Simulations are performed for this device to verify if the proposed design is suitable as a solar ratchet. Potential profiles are interesting along with current- and recombination-profiles of the devices. These give insight in the operation of the solar ratchet.

The program used is DriftKicker, introduced in chapter 0 'simulations'. To iterate, the program includes drift and diffusion currents, charge conservation, Coulomb interaction and the displacement current solved via forward integration in time after linearization of these equations. MatLab is the calculation program used to run DriftKicker.

4.4.1   Conventional solar cell simulation

A conventional organic solar cell is simulated to have a comparative basis against which a solar ratchet device can be evaluated. DriftKicker has been tested and used to simulate organic solar cells and therefore it is not needed to perform extensive program verifications. The left panel of Figure 34 shows a simulated IV-curve, i.e. current versus voltage, for a conventional solar cell. From this curve several device determined parameters vital to the efficiency of the solar cell are explained.

The already mentioned open circuit voltage is the 'drain' voltage at which the current of the solar cell vanishes. As has been explained V_{oc} is dependent on the difference between the quasi Fermi level of the holes in the donor and the quasi Fermi level of the electrons in the acceptor of the OPV. The difference between the band gap of the OPV and this V_{oc} is energy lost in the solar device. For the simulated solar cell the open circuit voltage is 0.5 eV.

The short circuit current is the current generated when the two contacts of the solar cell are shorted. This current is determined by the internal quantum efficiency of the device. Clearly you want this internal quantum efficiency, η, as large as possible. Amongst others η is determined by the electric field over the solar cell.

The third important characteristic of this IV curve is the so called fill factor. It is calculated to be the maximum power obtainable from the device divided by the product of the open circuit voltage and the short circuit current. The fill factor is ideally a 100% but for this solar cell it is in the order of 70%.
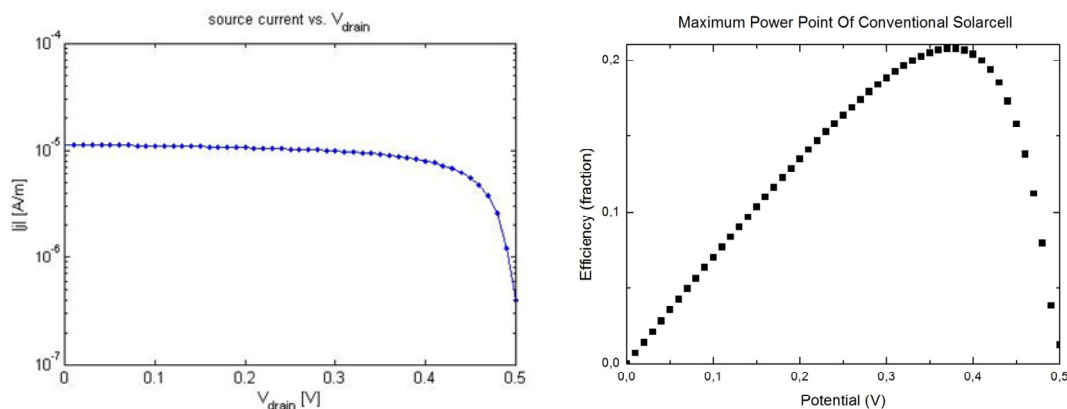

Figure 34 Simulation of a conventional solar cell with a bandgap of 1.2 eV and the work-function of the contacts of 4 and 5 eV. Left: IV curve for a conventional solar cell. Right: plot of the power efficiency vs drain voltage showing the maximum power point at 0.4 volt with an internal quantum efficiency of approximately 20%.

By combining the properties of this IV-curve we can calculate the power output and the power efficiency of the device. Here, the power efficiency is defined as the ratio of the power output of the device divided by the power generated in the device. This generated power is defined as the photon current multiplied by the bandgap of the device. In equations this looks as

$$P_{in} = I_{ph} \cdot V_{gap} \tag{11}$$

For this equation I_{ph} and V_{gap} are determined by the equations below.

$$I_{ph} = q \cdot G \cdot cl \tag{12}$$

$$q \cdot V_{gap} = E_{gap} = E_{LUMO}^{Acceptor} - E_{HOMO}^{Donor} \tag{13}$$

The photon current in the device is determined by the generation rate G times the elementary charge q and the length of the channel cl. The 'voltage' of the bandgap V_{gap} is the bandgap energy E_{gap} divided by the elementary charge q.

The efficiency at the maximum power point is slightly over 20%. The factors not included in this efficiency are the charge generation efficiency (the ratio of the number of free charges generated to the number of photons hitting the device) and the thermalization losses. The efficiency, short circuit current, open circuit voltage and fill factor give the necessary tools to evaluate the proposed solar ratchet.

4.4.2   Solar ratchet simulation method 1
The first simulation stage of the solar ratchet is done on a slightly different solar ratchet design as the one shown in Figure 33, the only difference is that single finger electrodes are present at the contacts which can be seen in Figure 35. These electrodes are meant to extract the charge carriers from the first and last subcell by creating electric fields in these subcells that are equal to those in the other subcells in the solar ratchet.
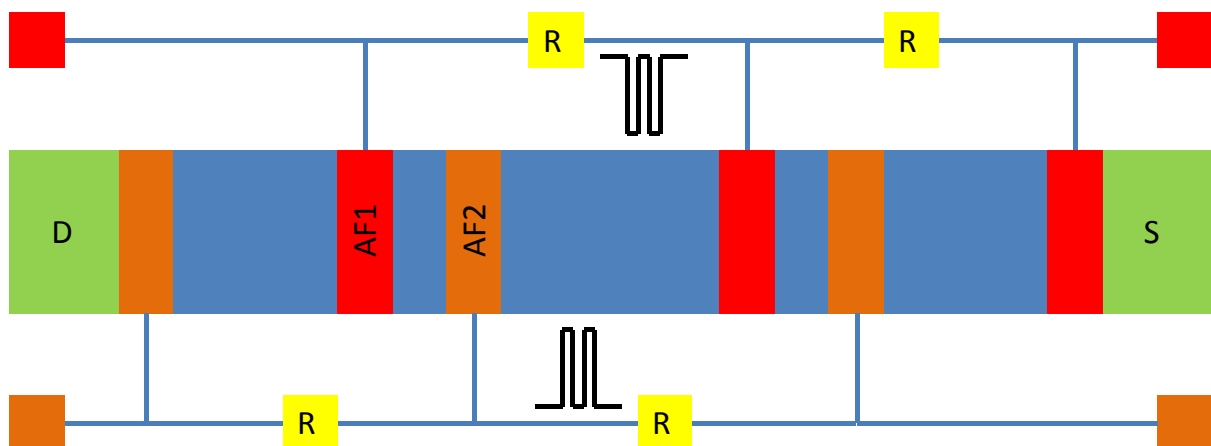

Figure 35 Solar ratchet with extra finger electrodes near the source and drain contacts to create an electric field on the first and last subcell equal to the electric field over the other subcells.

Figure 36 shows the IV-curve. When examined the V_{oc} immediately jumps out. There are three subcells in this system and when comparing this to the single conventional solar cell a V_{oc} of approximately 1.5 volt is expected, however a value of 10 volts is simulated. The calculated power efficiency on the right panel of Figure 36 shows a maximum of over 40%. This triggers a thorough investigation of the simulation.
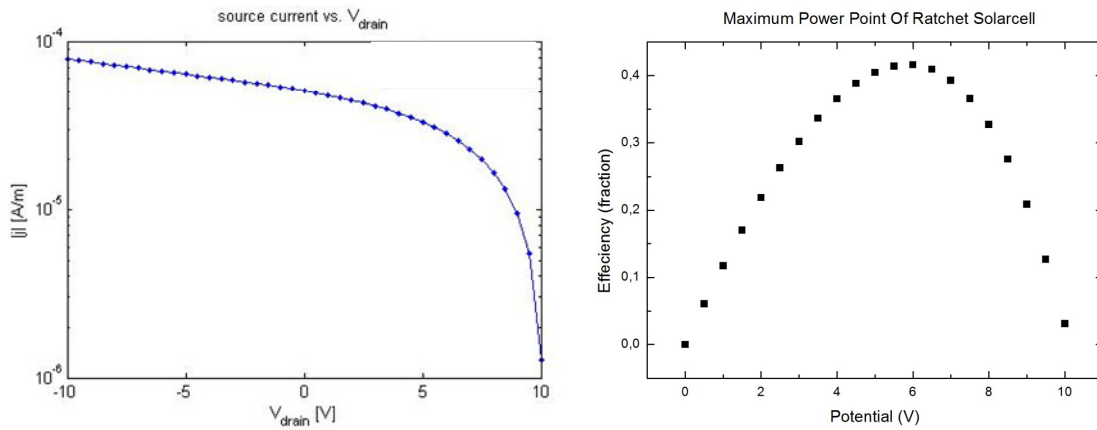

Figure 36 Simulation of a solar ratchet device with 3 finger electrode pairs where depending on the location of the finger electrodes a fraction of 20 or -20 V is placed. IV-curve of solar ratchet with an extremely high V$_{oc}$ of 10 V and a high current density of almost 10^{-4}A/m and a decent fill factor. This results in a very high efficiency of over 40% shown in the right panel. Unfortunately this cannot occur in a real device.

Figure 37 gives insight in the problem arising in the simulation. The potential profile of the channel of the solar ratchet is shown while the device is in operation with a 6 volt bias. Focusing at the huge potential step between zero and 500 nm in the device we can assume that the problems arise there. Electrons leave the device at that contact which means that they overcome an upward potential step of almost 6 volts. With the thermal energy being of the order of 25 millivolt, this is unrealistic.
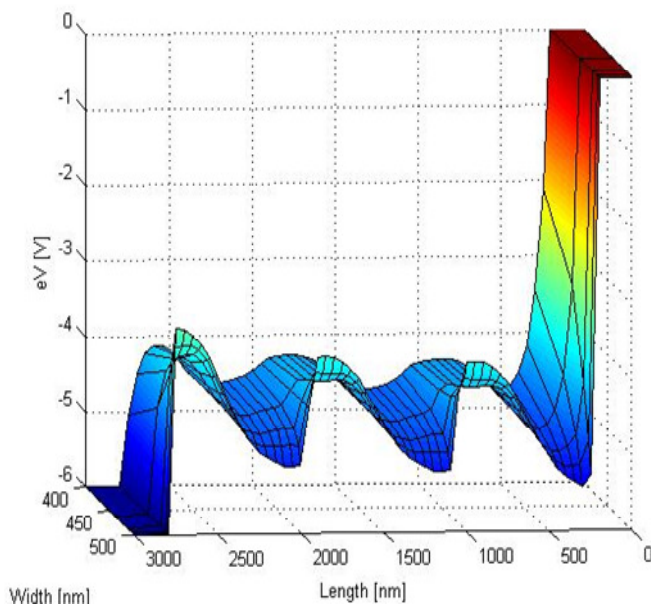
The question now is how the simulation does allow the charge carriers to overcome such a potential barrier. The answer lies in the way the currents are being calculated. In Figure 38 we go over the calculations looking at two side by side grid points on the calculation mesh. The potential *V* is displayed by the red line and the charge density *ρ* by the dark blue line. The diffusion current from site *i+1* to site *i* is of a finite value, from site *i* to *i+1* this diffusion current is zero. The drift current is expected to be the other way around, i.e. from *i* to *i+1*. The problem however is that at the time of calculating the charge density on site *i* is zero and therefore the drift current between *i* and *i+1* is zero. Combining both currents will result in a net current from site *i+1* to site *i* irrespective of the voltage difference.
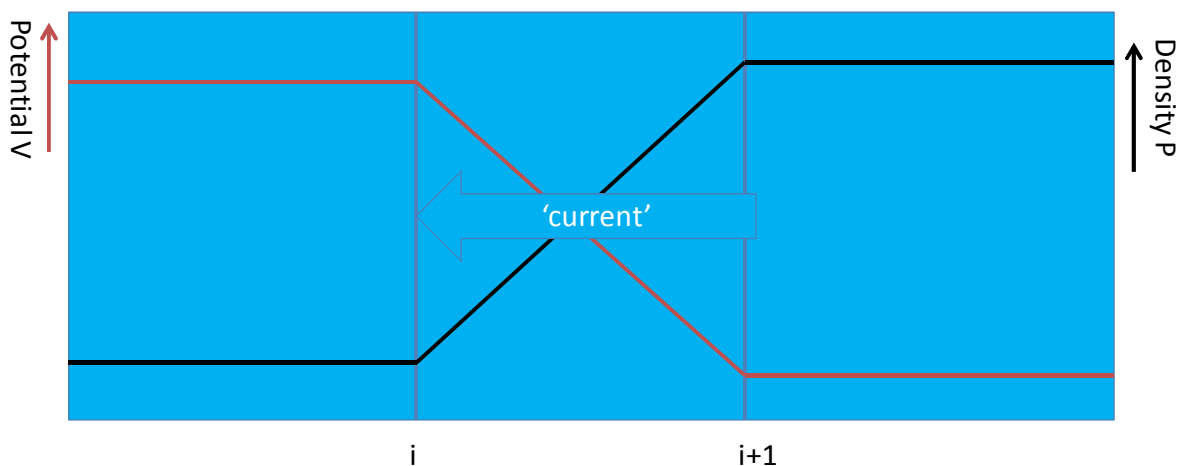

Figure 38 We look at 2 grid points in the calculations *i* and *i+1*. The current calculated in DriftKicker is directed from *i+1* to *i*. This happens because a finite diffusion current is calculated from *i+1* to *i* because of the gradient in density. The drift current from *i* to *i+1* is zero because there are no charge carriers available. These two currents are calculated sequentially and therefore there is not compensating current going back, resulting in a non physical current.

This is a fundamental problem of the 'separated' drift-diffusion simulation. Diffusion currents will be overestimated in the indicated extreme case. Undersampling does aggravate the problem but is not the cause of it. When simulations are done on a system where the finger electrodes at the contacts are removed and three finger electrode pairs are modeled with an increased number of grid points between the fingers the problem still occurs.

'Normal' electronic devices like solar cells and FETs do not run into this problem because this extreme potential profile does not exist in them. Recombination in tandem solar cells with the use of pn-junctions do run into this problem. They are however sparsely simulated and no literature has been found on this specific problem.

From Figure 39 the problem can be shown while looking at the potential in the channel of the device and the corresponding quasi Fermi levels of the electrons and the holes. In the middle panel we can see the quasi Fermi levels. At the recombination zones the Fermi level of the holes is higher than the Fermi level of the electrons, this is highlighted in the left panel. No recombination should occur because the holes and electrons are already in their respective potential minima, it however does for the same reason as above.
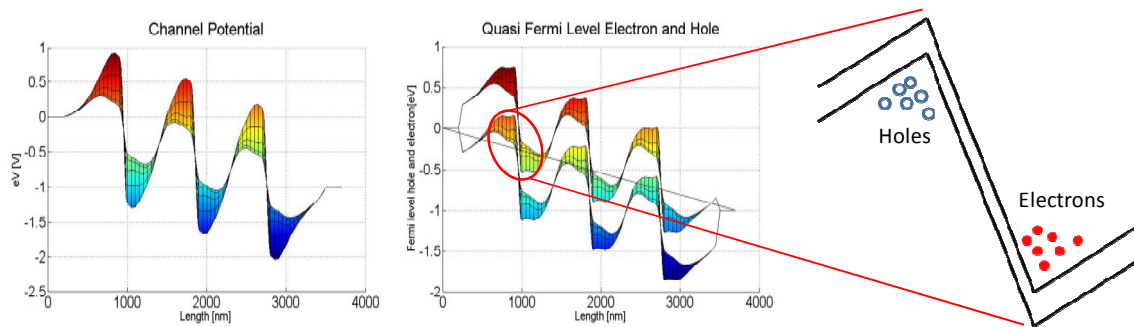
Figure 39 Simulated device is as in Figure 33 with three finger electrode pairs and a source-drain voltage of 1 V while the light is on. Left panel shows the potential profile of the semiconductor in the channel. In the middle the corresponding quasi Fermi levels are shown. Outlined is a schematic representation of what happens with the Fermi levels of the electrons and holes in the red encircled area. No recombination should be possible due to the higher Fermi energy of the holes in comparison to the Fermi energy of the electrons.

To deduce some information on the solar ratchet device from this type of simulations we assume that somehow recombination can exist on the intended positions. Note that we have just argued that this should not occur for the reasons above. We will come back to explain why we still do expect recombination.

The resulting IV-curve and the power as a function of the source-drain bias is shown in Figure 40. From the IV-curve we can see that the open circuit voltage is 2 volts. For four subcells this is the value that we would expect from adding the individual V_{oc} of 0.5 volts each.

The current and fill factor are bad for this particular device. The current from this device should consist of the electrons from the first subcell and the holes from the last subcell. To have the same quantum efficiency of a conventional solar cell the current has to be a factor 6 higher. It is however a factor 3 lower than in a conventional solar cell. The reason for this reduced current density is given later.

A high fill factor implies a very sharp decrease in the current near the open circuit voltage. Here, it gradually decreases, leading to a fill factor of 25%. Combining these factors leads to a low power and a very low efficiency as can be seen in the right panel of Figure 40.
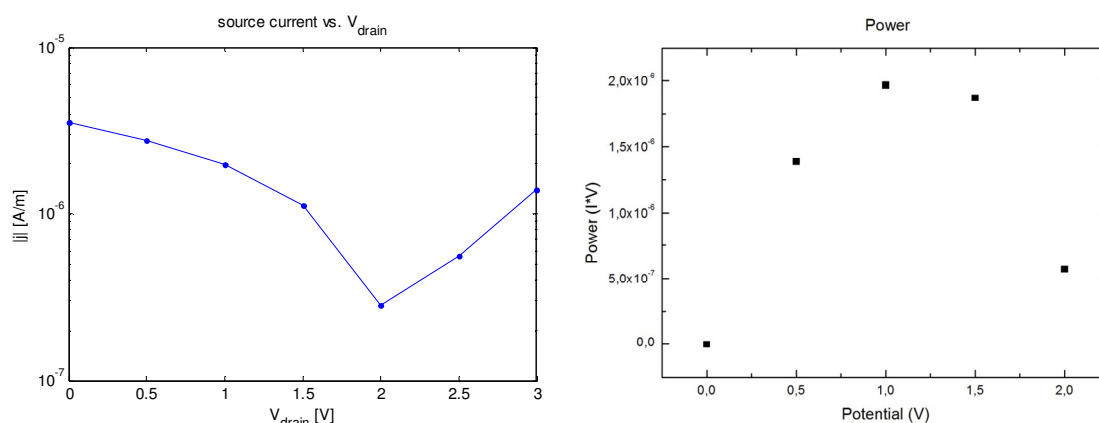

Figure 40 Simulation of a solar ratchet device where 4 finger electrode pairs with depending on the location of the finger electrodes a fraction of 20 or -20 V is placed. Left: IV-curve of a solar ratchet. Right: power curve for this IV-curve showing low power output of the device. An approximate recombination strength is used.

Again if this recombination is possible we can investigate how the charge carriers behave in the channel. Figure 41 shows quasi Fermi levels, the recombination profile and the electron and hole currents. From the quasi Fermi levels the increase in V_{oc} is displayed with the recombination occurring in the designated recombination zones.

In the bottom two panels the electron and hole currents are visualized. Here we can see that the electrons and holes have difficulty getting out of the device because no current densities are found near the contacts. The reason for this is that the work function of the contacts are taken mid bandgap. Ideally the workfunction of the contacts are near the Fermi levels of respectively the acceptor LUMO level and the donor HOMO level. In this case a higher fill factor and current is expected, resulting in a better power efficiency.
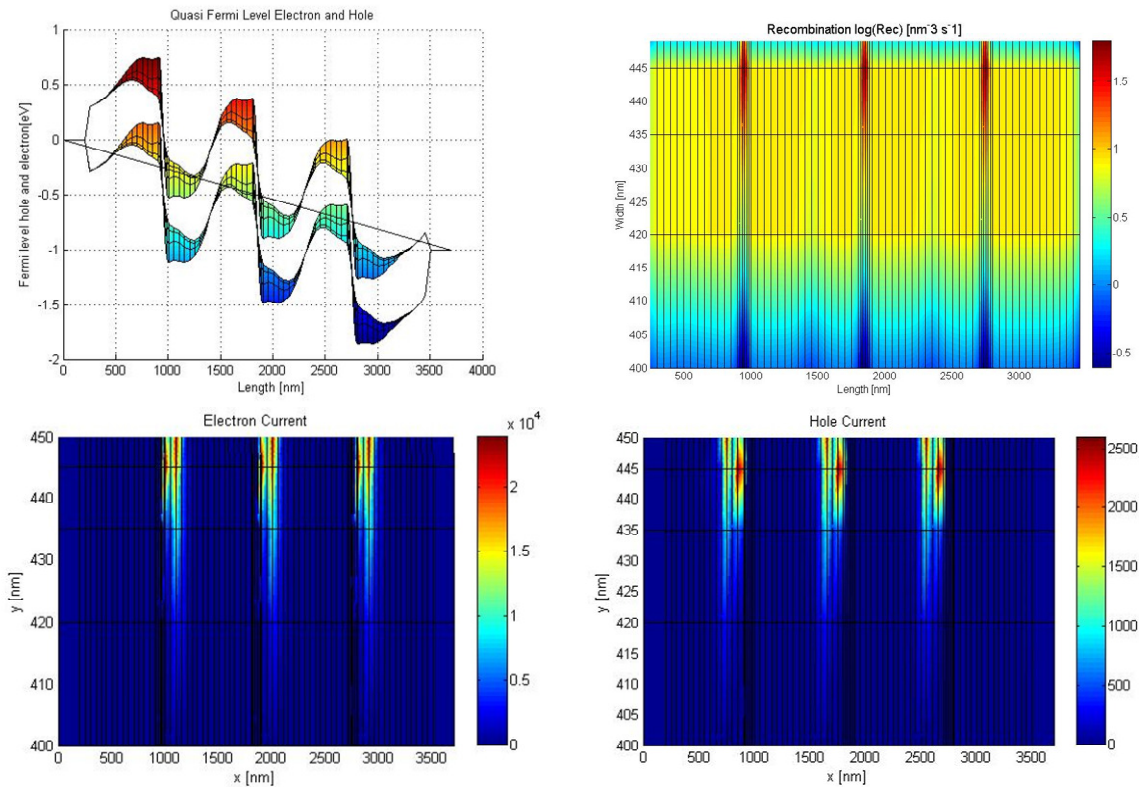

Figure 41 Intended working of an organic solar ratchet. The quasi Fermi levels in the top left panel remind the position of the recombination areas. The top right panel shows the recombination which occurs exactly at the predetermined zones. The two bottom panels show the hole and electron current for which the currents near the recombination zones are high, but the current moving into the contacts are small. Note that where the electron and hole currents come close to each other recombination takes place.

4.4.3 Solar ratchet simulation method 2

A second simulation method is used to solve the problem of recombination occurring while being energetically forbidden, as was shown in Figure 39. Transport of charge carriers is now calculated with the Boltzmann transport equation:

$$j^n = -q\mu_e n\nabla\Psi_{F,n}. \tag{14}$$

Here j^n is the electron current, q the elementary charge, μ_e the electron mobility, n the electron density and $\nabla\Psi_{F,n}$ the gradient of the chemical potential or Fermi energy.

This equation replaces the drift-diffusion equation in chapter 0 'simulations'. The difference between the two methods is that in the drift-diffusion equation the current components are being calculated separately which caused the carriers to be transported 'uphill' in energy.

In the Boltzmann transport equation drift and diffusion currents are simultaneously calculated from the gradient in the Fermi energy.

First the same simulations as were performed by method 1 were repeated. A full solar ratchet is simulated with the exact geometry as described in Figure 33. However recombination of the current at aforementioned zones is not allowed in this simulation. The reason that there is no recombination in this second version of the simulation is simply because there is no mechanism simulated that allows recombination. For the implemented equations recombination will only occur if electrons and holes arrive on the same grid point and are not transported away again. This will not happen because the Boltzmann transport equation does not allow the charge carriers to reach the recombination zone between the finger electrodes: the spurious mechanism explained in Figure 41 is no longer operational.

It is however not futile to look at this new simulation method. In a pn-junction used as recombination layer in a conventional tandem cell recombination does occur. Important in such a zone is the depletion length of the pn-junction. This depletion length is the distance over which no free holes and electrons are available. The fact that recombination does occur implies that electrons and holes somehow do make it across this depletion zone.

Determination of the depletion length in a ratchet-type device is done by simulation of a single finger electrode pair with two contacts at a distance of 600 nm. The distance between the finger electrodes is again 100 nm. This region is divided in 50 times 2 nm grid points. This system is left at short-circuit to find its quasi steady-state.

The potential profile in the channel for this quasi steady-state is shown in the left panel of Figure 42. From this figure we can deduce that the potential drop between the finger electrodes occurs over a range of approximately 8 grid cells, this corresponds to 16 nm. The same holds for the position of the holes and the electrons in the middle and right panel. Therefore the depletion length of the junction in the recombination zone is of the order of 10 to 20 nm[34].

This depletion length is much shorter than the short finger distance of 100 nm. This is the result of the Coulomb interaction between the holes and electrons accumulated at the finger electrodes. This Coulomb interaction forces the charge carriers to get close to each other. The distance between the electrons and holes can also be found in Figure 42 (B) and (C).
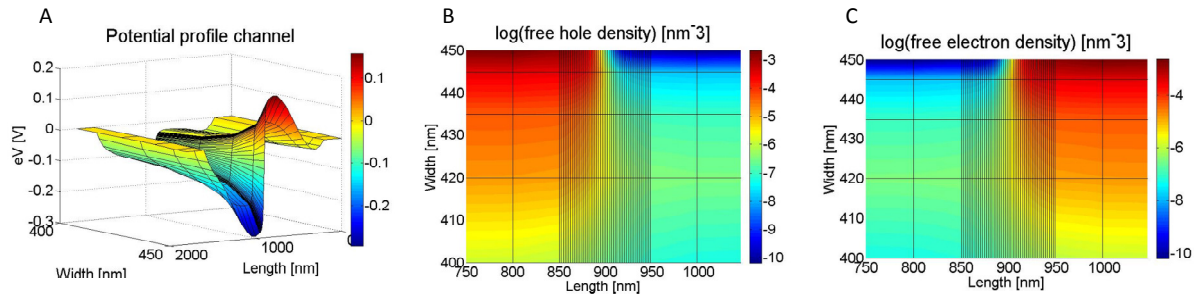
Figure 42 Simulation of single finger electrode pair between two contacts with 50 grid-points between the two finger electrodes. Simulation method two showing the depletion length of the recombination zones in a solar ratchet. This is determined by investigating the potential drop, and the position of the free holes and electrons in the device. Found to be approximately 8 grid cells corresponding to 16 nm.

4.4.4   pn-junction in tandem solar cell

In version 1 of the simulations the transport of charge carriers against the potential is overestimated because of the separate calculation of the drift and diffusion currents. This results in recombination in the zones designed for the charge carriers to recombine. Figure 39 shows why this recombination should mathematically not be possible.

In version 2 no recombination occurs as is described in the previous section. However the depletion length of the system is determined.

The depletion region created in the channels is however not different from the situation in the pn-junction in a tandem solar cell. These junctions in tandem solar cells are known to work well. The recombination mechanism in these junctions may shed some light on the present problem in simulations of solar ratchets.

The principle of tunnel diodes is used in the tandem solar cells with recombination layers consisting of pn-junctions. Two different principles of recombination can be introduced to explain why these pn-junctions work as recombination zones.

First Zener tunneling[35] can be the principle behind this recombination. It states that in semiconductors charge carriers can tunnel trough the barrier formed by the bandgap if the field is sufficiently large, i.e. if the depletion length of these barriers is small. The tunneling length is schematically drawn in the left panel of Figure 43, the maximum length of this barrier may be in the order of 10 to 20 nm[34].
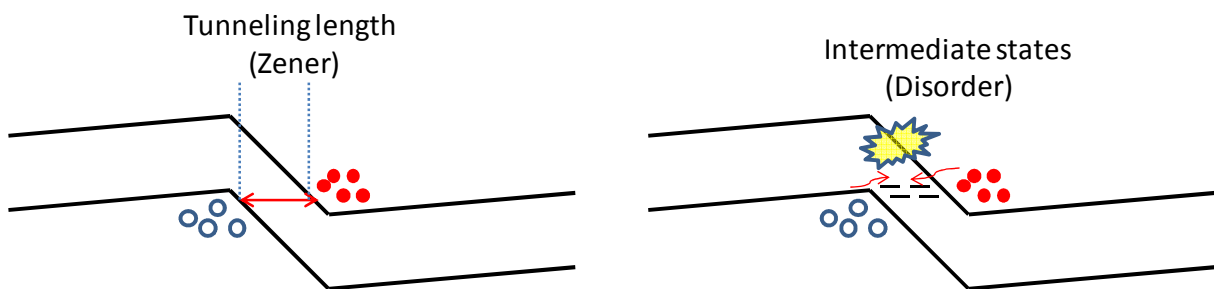

Figure 43 Left panel: Zener tunneling; in a semiconductor layer (red) electrons can recombine with (blue) holes if the tunneling length (red double headed arrow) is not too long. Right panel: intermediate states in the recombination zone cause recombination to occur because holes as well as electrons can move towards each other. This facilitates Langevin recombination.

Secondly intermediate states[36] can also facilitate recombination in pn-junctions. These intermediate states might arise due to disorder and create the possibility to transport charge carriers directly towards each other without the need to tunnel over large distances. The schematic interpretation of this process can be found in the right panel of Figure 43.

Zener tunneling and intermediate states are not included in the simulation program DriftKicker which will therefore not show any recombination currents when properly ran. The strong analogy between working pn-junctions in tandem solar cells and theorized solar ratchet devices with recombination layers created with finger electrodes is hopeful that recombination can occur.

4.5   Towards proof of principle

From the simulations done with DriftKicker in the previous chapter and the following discussion on recombination it can be assumed that these solar ratchet devices will work. However no proof is given for this claim and it is only made plausible through the use of analogies to already existing devices. The groundwork for these devices has been done and gives strong indications that the design made in Figure 33 is suitable for use as a solar ratchet. Simulations show that the device can work as intended when recombination in the therefore designed zones is (so far artificially) made possible.

To extrapolate this research two things can be done. Simulations can be extended to include these recombination processes and/or a proof of principle can be made. In this thesis only the second option is chosen. To implement the recombination processes in the DriftKicker simulation is chosen to be beyond the scope of this research.

Two different paths to creating a proof of principle are made. First it will be tried using a standard organic electronic ratchet while the organic semiconductor is an OPV. The second attempt will be to make the design in Figure 33 from scratch and measure the full potential of this first attempt of creating a solar ratchet.

4.5.1   Proof of principle from an organic electronic ratchet

When the semiconducting layer of an organic electronic ratchet is substituted for an OPV material it can function as a solar ratchet at short circuit.

This ratchet does not contain all the characteristics of a in this section proposed solar ratchet. As stated in the organic electronic solar ratchet section, the gate electrode prohibits the V_{oc} to build up over the channel. This is not a problem because the pairs of finger electrodes cannot be put at different offset biases to create the desired stepwise increment introduced in Figure 33. This device can however produce a short circuit current. P3HT/PCBM is chosen as the photovoltaic because it is a stable material which is easily available.

The short circuit current originates from the first and last subcell of the solar ratchet. For the current to run recombination needs to occur at the therefore designed zones. Therefore this proof of principle would prove the claim that the analogy with pn-junctions in a tandem solar cell is justified.

For two different cases this device was tested.

First the original organic electronic ratchet design is tested. No current was detectable over the noise level. The likely explanation for this is that the recombination zones are much wider here, 1 μm between two finger electrodes, instead of the 100 nm wide recombination zones designed for the solar ratchet.
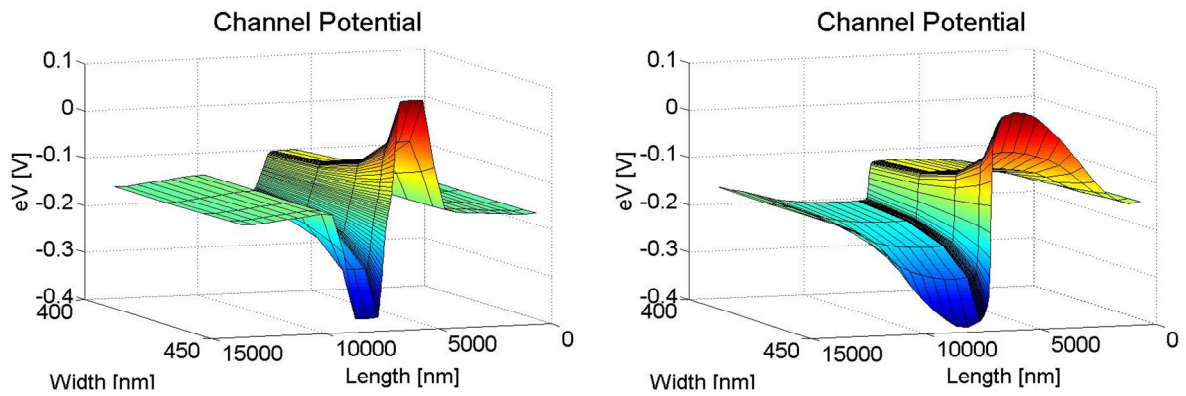
Figure 44 Channel potentials with on the left the potential for a ratchet device with 100 nm SiO$_2$ between the finger electrodes and the semiconducting layer and a potential of 20 and -20 V on the finger electrodes. On the right a ratchet device with 1000 nm SiO$_2$ and a potential of 200 and -200 V on the finger electrodes. The depletion length is a lot smaller while the absolute potential remains the same.

Next, to try to facilitate the recombination of holes and electrons in these zones the spacing between the finger electrodes and the OPV is increased to 1 µm. This spacing is introduced to help the electrons and holes to come closer to each other under the influence of their Coulomb interaction. This can be seen in Figure 44. Each grid point on the calculation mesh is 20 nm apart and in the device on the left, with 100 nm of SiO$_2$ between the OPV and the finger electrodes, the holes and electrons are separated by many grid points. On the right this is only a few points and which could potentially be close enough for recombination. Here the OPV and the finger electrodes are the proposed 1 µm apart with SiO$_2$ in between.

Unfortunately this also did not result in a measurable current. The created recombination zone of 1 µm is possibly still too wide for the electrons and holes to effectively attract each other. Therefore the depletion length of the recombination zones remains very large and Zener tunneling or intermediate disorder states cannot enable efficient recombination.

4.5.2   Proof of principle from scratch

The solar ratchet design presented in Figure 33 is best suitable to create an experimental proof of principle. This design can be fabricated in several ways. Here the use of electron beam lithography (EBL) is chosen. The fabrication process is described in chapter 3.6 'fabrication process'.

The choice for EBL is made for its flexibility towards different designs and the small feature sizes it can reach. It is therefore possible to test many slightly different designs, enabling (potentially) several iterations of the devices.

First test lines are made, which are used to determine the settings of the EBL machine used for electron beam lithography. After 3 iterations the lines are good enough to proceed to try to make parts of the total structure, visible in Figure 45. Panel (A) shows four straight lines of 100 nm with less than 100 nm in between two lines and panel (B) shows 2 corners tested to be open in between the two lines. The settings used for these samples are an aperture of 7.5 μm, an acceleration voltage of 20 kV and a dose of 180 μC/cm^2.
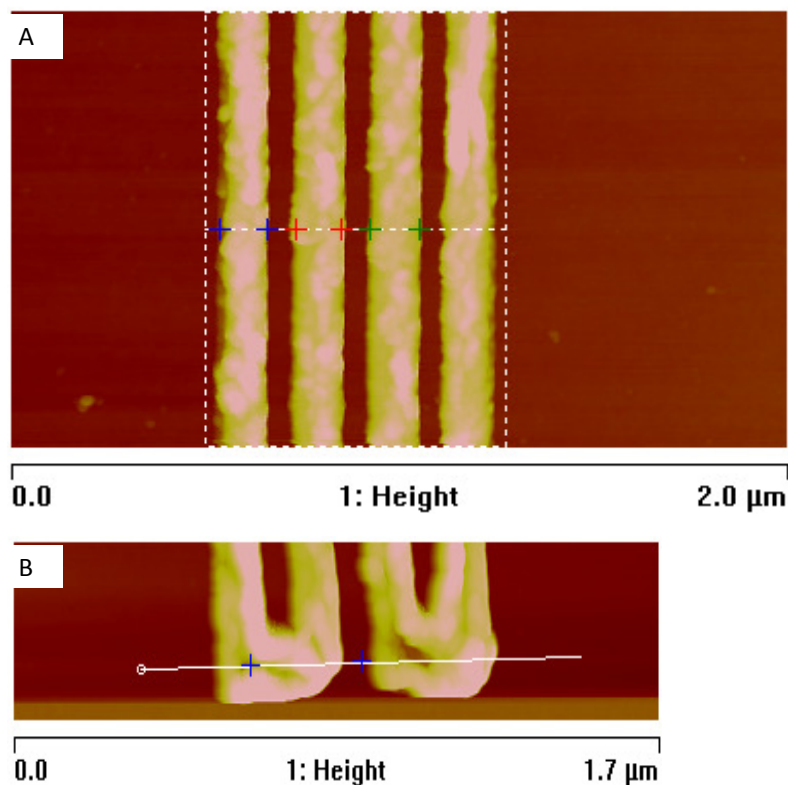

Figure 45 Test lines designed to investigate the best settings of the machine used for EBL. Lines approximately 100 nm in width and 50 nm in between.

Increasing or decreasing the aperture changes the possible feature sizes that can be made. The acceleration voltage determines parameters like back scattering from the substrate and the dispersion of the initial beam. The dose is set by the duration of the beam on a single location. It determines the level of exposure of the resist.
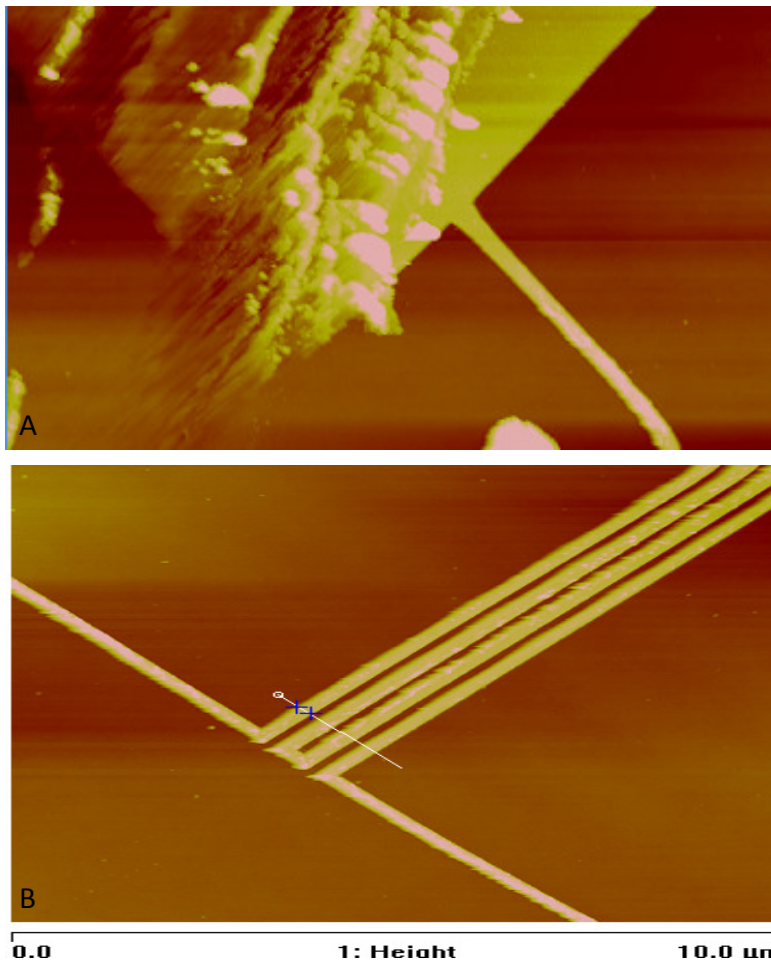
Figure 46 panel A shows the connection between the finger electrodes to the contact after contacting the contact pad with a probe needle. Panel B shows part of the structure of a solar ratchet device, the resistive path.

Figure 46 shows the results of trying to make different parts of the total structure. Panel (A) shows the point at which a finger, source or drain electrode reaches the contact pad. A probe needle has previously been placed onto this contact pad. The finger electrode coming from the contact is still in place.

On basis of this very promising result we have tried to make a full solar ratchet. Figure 47 shows a typical result. The quality of the lines turned out to be very bad. Part of the structure was made again and every time bad results were obtained.

The parameter settings determined in the production of single lines were reevaluated but no particular setting created the desired result. Therefore it was unfortunately impossible to create a proof of principle from scratch.
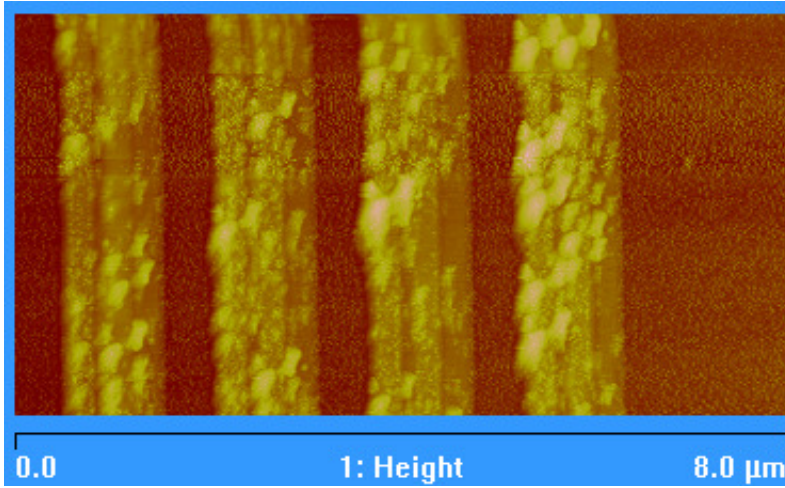
Figure 47 Part of a full solar ratchet. Four resistive paths should be visible in this picture. The individual resistive paths are clumped together. The settings are identical to the ones used for Figure 46.

5   Conclusion

Two main topics have been investigated in this thesis. The (in)organic electronic ratchet and the organic solar ratchet. Both topics resulted in remarkable results.

5.1   Organic electronic ratchets

For organic electronic ratchets three subsections can be made. The driving mechanisms behind the electronic ratchet, the scaling mechanism of the electronic ratchet as a function of the frequency, and the unexpected IGZO current reversals. The conclusions of these sections are represented here.

First the principle behind the ratchet is shortly explained. Symmetry breaking and creating an out-of-equilibrium state are essential to drive current. The basic principle is easy but becomes hard to fully understand when the investigated ratchet becomes more complex because of multiple asymmetries, related to both the driving signal and the geometry.

The first picture used to comprehend the driving of current in an electronic ratchet is the on/off ratchet which explains the net current in case of an electronic ratchet driven with a forward or reverse driving signal with a phase difference of 180 degrees between the two sets of finger electrodes. The picture needs to be extended to include charge waves and their nonlinear interference. This intuitively explains the currents and their reversals as a function of the phase and frequency of the driving signal. For quantitative understanding the model becomes more complex because of the different length scales that play a role, i.e. the influence of the long, short, and total length of the ratchet.

Second the scaling properties as a function of frequency are investigated. The current vs. phase and frequency was found to be linearly dependent on the mobility of the charge carriers. These mobilities can therefore be scaled out of the result, creating a universal profile as function phase and frequency where the latter is normalized by the RC-time of the device. This profile is independent of the semiconductor material. No dependency on either positive or negative charge carriers is found, other than the expected reversal of the current. Furthermore no influence has been found on the nature, organic/inorganic, of the semiconductor. This resulted in coherent scaling of the current profile as a function of the frequency for up to seven orders of magnitude.

At last, for IGZO peculiar currents and current reversals have been found for low frequency driving signals. The charge per cycle of these currents is two orders of magnitude larger than expected from simulations. The nature of these currents is not related to drift effect; rather it appears to be a diffusion current. This is however still uncertain.

5.2   Organic electronic solar ratchets

Regarding the second main topic solar ratchets were designed and tested. This lateral device was designed to generate current as a solar cell with the aim to generate an open circuit voltage that equals, or exceeds, that of a single cell times the number of repeat units of the ratchet potential.

The combined result of two versions of simulations show that the device should work not unlike a tandem solar cell with recombination zones in the form of a pn-junction. This cannot be directly tested because the used simulation models lack a correct description of the recombination process in these devices.

It was tried to make a proof of principle from both the existing ratchet design and from a specially designed layout. The proof of principle from an existing ratchet design did not result in any current being detected over the noise limit.

The specially designed structure was not produced in the timeframe of this graduation project. Electron beam lithography problems prohibited the fabrication of a complete solar ratchet device, although promising test structures were made. The design should however result in a working solar ratchet creating a current with an open circuit voltage of several times the open circuit voltage of a conventional solar cell.

Unfortunately the simulated (approximate) efficiency of this solar ratchet is small; the device is therefore unlikely to compete with a conventional solar cell.

6 References

[1] Smoluchowski, M. v. Experimentell nachweisbare, der üblischen Thermodynamik widersprechende Molekularphänomene. Physikalische Zeitschrift 13, 1069-1080

[2] Feynman, R. P., Sands, M. L. & Leighton, R. B. the feynman lectures on physics. (Addison-Wesley, 1989)

[3] E.M. Roeling, Organic electronic ratchets, thesis 2011, 123, 978-90-386-2468-6

[4] Reiman, P. Brownian motors: noisy transport far from equilibrium. Physics Reports-Review Section of Physics Letters 361, 57-265, (2002)

[5] Ferruccio Renzoni, Chapter 1 Driven Ratchets for Cold Atoms, In: E. Arimondo, P. R. Berman and C. C. Lin, Editor(s), Advances In Atomic, Molecular, and Optical Physics, Academic Press, 2009, Volume 57, Pages 1-32, ISSN 1049-250X, ISBN 9780123747990

[6] N. Pamme, Continuous flow separations in microfluidic devices, Lab Chip, 7, 1644-1659, 2007

[7] van Oudenaarden, A. & Boxer, S. G. Brownian ratchets: Molecular separations in lipid bilayers supported on patterned arrays. Science 285, 1046-1048, (1999)

[8] Linke, H. et al. Self-propelled Leidenfrost droplets. Phys Rev Lett 96, 154502, (2006)

[9] Loutherback, K., Puchalla, J., Austin, R. H. & Sturm, J. C. Deterministic Microfluidic Ratchet. Phys Rev Lett 102, 045301, (2009)

[10] Mahut, G. et al. Directing cell motions on micropatterned ratchets. Nature Physics 5, 606-612, (2009)

[11] Grimm, A. SEPARATION AND COLLECTIVE PHENOMENA OF COLLOIDAL PARTICLES IN BROWNIAN RATCHETS. A THESIS SUBMITTED FOR THE DEGREE OF DOCTOR OF PHILOSOPHY. National university of Singapore, (2010)

[12] Sze, S. M. & Ng, K. K. physics of semiconductor devices. 3rd edn, (Wiley-Interscience, 2007)

[13] Horowitz, G., Hajlaoui, R., Bouchriha, H., Bourguiga, R. & Hajlaoui, M. The concpept of 'threshold voltage' in organic field-effect transistors. Adv Mater 10, 923-927, (1998)

[14] Bobbert, P.A. et al. Operational Stability of Organic Field-Effect Transistors. Advanced Materials 24-9, 1146-1158 (2012)

[15] Roeling, E.M. et al. Scaling of characteristic frequencies of organic electronic ratchets. Phys Rev B 85, 045430 (2012)

[16] Roeling, E. M. et al. Organic electronic ratchets doing work. Nat Mater 10, 51-55, (2011)

[17] Linke, H. et al. Experimental tunneling ratchets. Science 286, 2314-2317 (1999)

[18] For a review see: Hanggi, P. & Marchesoni, F. Artificial Brownian motors: Controlling transport on the nanoscale. Rev Mod Phys 81, 387-442 (2009)

[19] For a review see: Reimann, P. Brownian motors: noisy transport far from equilibrium. Physics Reports-Review Section of Physics Letters 361, 57-265 (2002)

[20] Silva, C. C. D., de Vondel, J. V., Morelle, M. & Moshchalkov, V. V. Controlled multiple reversals of a ratchet effect. Nature 440, 651-654 (2006)

[21] Coehoorn, R., Pasveer, W. F., Bobbert, P. A. & Michels, M. A. J. Charge-carrier concentration dependence of the hopping mobility in organic materials with Gaussian disorder. Phys Rev B 72, 155206, (2005)

[22] Holst van der, J. J. M., Oost van, F. W. A., Coehoorn, R. & Bobbert, P. A. Electron-hole recombination in disordered organic semiconductors: Validity of the Langevin formula. Phys rev B 80, 235202, (2009)

[23] Roeling, E. M., Germs W., Kemerink, M. Organische electronische ratchets NtvN, (2011)

[24] Balocco, C., Majewski, L. A. & Song, A. M. Non-destructive patterning of conducting-polymer devices using subtractive photolithography. Org Electron 7, 500-507, (2006)

[25] Constancias, C., Landis, S., Manakli, S., Martin, L., Pain, L. and Rio, D. Electron Beam Lithography, in Lithography (ed S. Landis), John Wiley & Sons, Inc., Hoboken, NJ USA. (2013)

[26] Tang, C. W. A two-layer organic solar cell. Appl. Phys. Lett. 48, 183-185 (1986)

[27] Yu, G., Zhang, C. & Heeger, A. J. Dual-function semiconducting polymer devices: light-emitting and photodetecting diodes. Appl. Phys. Lett. 64, 1540-1542 (1994)

[28] Yu, G., Gao, J., Hummelen, J., Wudl, F. & Heeger, A. J. Polymer photovoltaic cells-enhanced efficiencies via a network of internal donor-acceptor heterojuncitons. Science 270, 1789-1791 (1995)

[29] Peumans, P., Uchida, S. & Forrest, S. R. Efficient bulk heterojunction photovoltaic cells using small-molecular-weight organic thin films. Nature 425, 6954, 158-162 (2003)

[30] Eersel van, H., Janssen, R. A. J., Kemerink, M. Mechanism for efficiënt photoinduced charge separation at disordered organic heterointerfaces. AdvFuncMat (2012)

[31] http://www.nanochemistry.it/download/download.html

[32] Gilot, J., Wienk, M. M., Janssen, R. A. J. Optimizing Polymer Tandem Solar Cells. AdvMat 22, 67-71, (2010)

[33] Timmreck, R., Olthof, S., Leo, K. & Riede, M. K. Highly doped layers as efficiënt electron-hole recombination contacts for tandem organic solar cells. J. Appl. Phys. 108, 033108, (2010)

[34] Blochwitz, J., Fritz, T., Pfeiffer, M., Leo, K., Alloway, D. M., Lee, P. A., Armstrong, N. R. Interface electronic sturture of organic semiconductors with controlled doping levels. Org Elec 2,97-104, (2001)

[35] Fröbel, M., Permual, A., Schwab, T., Gather, M. C., Lüssem, B., Leo, K. Enhancing the efficiency of alternating current driven organic light-emitting devices by optimizing the operation frequency. Org Elec 3, 809-813, (2013)

[36] Sah, R.L-Y., Noyce, Robert N, Shockley, William, Carrier Generation and Recombination in P-N Junctions and P-N Junction Characteristics. *Proceedings of the IRE* , vol.45, no.9, pp.1228-1243, Sept. 1957